General Disclaimer

One or more of the Following Statements may affect this Document

- This document has been reproduced from the best copy furnished by the organizational source. It is being released in the interest of making available as much information as possible.

- This document may contain data, which exceeds the sheet parameters. It was furnished in this condition by the organizational source and is the best copy available.

- This document may contain tone-on-tone or color graphs, charts and/or pictures, which have been reproduced in black and white.

- This document is paginated as submitted by the original source.

- Portions of this document are not fully legible due to the historical nature of some of the material. However, it is the best reproduction available from the original submission.

AD-783 538

THE MAGNETOSPHERE OF JUPITER AS OBSERVED WITH PIONEER 10. PARTS I, II, AND III

J. A. Van Allen, et al

Iowa University

AD 783 538

REPORT DOCUMENTATION PAGE	READ INSTRUCTIONS BEFORE COMPLETING FORM

1. REPORT NUMBER	2. GOVT ACCESSION NO.	3. RECIPIENT'S CATALOG NUMBER

4. TITLE (and Subtitle)	5. TYPE OF REPORT & PERIOD COVERED
THE MAGNETOSPHERE OF JUPITER AS OBSERVED WITH PIONEER 10. Parts I, II, and III	Progress May 1974
	6. PERFORMING ORG. REPORT NUMBER

7. AUTHOR(s)	8. CONTRACT OR GRANT NUMBER(s)
Various (See abstracts on reverse side)	N00014-68-A-0196-0009

9. PERFORMING ORGANIZATION NAME AND ADDRESS	10. PROGRAM ELEMENT. PROJECT, TASK AREA & WORK UNIT NUMBERS
Department of Physics and Astronomy The University of Iowa Iowa City, Iowa 52242	

11. CONTROLLING OFFICE NAME AND ADDRESS	12. REPORT DATE
Office of Naval Research Arlington, Virginia 22217	May 1974
	13. NUMBER OF PAGES
	~~126~~ 127

14. MONITORING AGENCY NAME & ADDRESS(if different from Controlling Office)	15. SECURITY CLASS. (of this report)
	UNCLASSIFIED
	15a. DECLASSIFICATION/DOWNGRADING SCHEDULE

16. DISTRIBUTION STATEMENT (of this Report)

Approved for public release; distribution is unlimited.

17. DISTRIBUTION STATEMENT (of the abstract entered in Block 20, if different from Report)

18. SUPPLEMENTARY NOTES

To be published in Journal of Geophysical Research

19. KEY WORDS (Continue on reverse side if necessary and identify by block number)

Pioneer 10
Planetary magnetospheres
Jupiter

20. ABSTRACT (Continue on reverse side if necessary and identify by block number)

[See page following.]

127

DD FORM 1473 EDITION OF 1 NOV 65 IS OBSOLETE
1 JAN 73
S/N 0102-014-6601 |

i.

THE MAGNETOSPHERE OF JUPITER AS OBSERVED WITH PIONEER 10

Part I: Instrument and Principal Findings
          J. A. VAN ALLEN, D. N. BAKER, B. A. RANDALL, and D. D. SENTMAN

20.   Abstract

This paper reports on the first in situ observations of energetic electrons of energy $E_e > 0.06$ MeV in the magnetosphere of Jupiter during November-December 1973. The outer magnetosphere has the form of a thin disc-like, quasi-trapping region extending from about 20 to over 100 R_J (planetary radii). This magnetodisc is confined near the magnetic equatorial plane and has approximate axial symmetry about the magnetic axis of the planet. The observations inside a radial distance of 12 R_J are well organized by a centered dipolar model of the planet's magnetic field with a tilt of $9^\circ.5 \pm 0^\circ.5$ to the rotational axis and with pole at a System III longitude of $230^\circ \pm 3^\circ$. Absolute omnidirectional intensities of electrons within the stable trapping region inside 20 R_J are given for four energy ranges $E_e > 0.06, > 0.55, > 5.0, > 21,$ and > 31 MeV. One example is

$$J \, (E_e > 21 \text{ MeV}) = 3.0 \times 10^8 \exp\left(-L/1.45\right) \left(\frac{\cos^6 \Lambda}{\sqrt{4 - 3\cos^2 \Lambda}} \right)^{m/2}$$

for $3.5 < L < 12$ R_J, where J is in electrons/cm^2 sec, L is the magnetic shell parameter in units of R_J, and Λ is the magnetic latitude. The pitch angle parameter $m = 3.5 + (3.86/L)^8$. Marked depletion of particle intensities at the orbits of Io, Europa, and Ganymede is observed in the lower energy ranges.

Part II: Non-Rigid Rotation of the Magnetodisc
           C. K. GOERTZ, T. G. NORTHROP, and M. F. THOMSEN

20.   Abstract

The maximum count rates of energetic particles are observed earlier on the inbound pass and later on the outbound pass than one would expect if the Jovian magnetodisc rotated rigidly with the planet. This lead and lag cannot be explained by the observed azimuthal distortion of the Jovian magnetic field alone. The foot of a magnetic field in the ionosphere must slip with respect to Jupiter's surface. The rate of slippage and the electric field necessary for this is estimated. The electric field may be as large as 2 volts/meter in the Jovian polar ionosphere.

Part III: Jovian Synchrotron Radiation at 10.4 cm as Deduced from Observed
           Electron Fluxes
           T. G. NORTHROP and T. J. BIRMINGHAM

20.   Abstract

Synchrotron radiation at 10.4 cm wavelength between 2.9 and 5.0 Jovian radii has been calculated from the electron fluxes observed by the Iowa Pioneer 10 detectors. This calculated emissivity (watts/m^3 x Hz x steradian) exceeds the Beard-Luthey [1973] spatial resolution of the Berge [1966] interferometer measurements by about a factor of 2 at 3 Jovian radii. The calculated emissivity is quite insensitive to the energy spectral index. It is only moderately sensitive to the equatorial angular distribution. The disagreement would be only about 30% if Beard and Luthey had used the Iowa angular distribution. A factor of 2 would represent a genuine disagreement, but 30% would not exceed the combined uncertainties of our analysis and the Beard-Luthey analysis.

2.

THE MAGNETOSPHERE OF JUPITER

AS OBSERVED WITH PIONEER 10

Part I: Instrument and Principal Findings
J. A. VAN ALLEN, D. N. BAKER, B. A. RANDALL,
and D. D. SENTMAN

Part II: Non-Rigid Rotation of the Magnetodisc
C. K. GOERTZ, T. G. NORTHROP, and M. F. THOMSEN

Part III: Jovian Synchrotron Radiation at 10.4 cm as
Deduced from Observed Electron Fluxes
T. G. NORTHROP and T. J. BIRMINGHAM

Department of Physics and Astronomy
The University of Iowa
Iowa City, Iowa 52242

May 1974

2a

INTRODUCTION

The University of Iowa instrument on Pioneer 10 is a modified version of one proposed in November 1968. The original design was simplified and revised in accordance with constraints specified by the National Aeronautics and Space Administration at the time of acceptance of the experiment in early 1969.

Among the several observational objectives of our experiment, the principal one was to make an exploratory survey of the absolute intensities, energy spectra, and angular distributions of energetic electrons and protons as a function of position along the trajectory of the spacecraft through the magnetosphere of Jupiter, giving primary emphasis to electrons of energy $E_e > 0.06$ MeV and secondary emphasis to protons of energy $E_p > 6.6$ MeV.

A preliminary report of our Jovian encounter measurements has been published [Van Allen et al., 1974a, 1974b]. The present paper is based on a thorough re-analysis of detector calibrations and of the observational data.

DESCRIPTION OF INSTRUMENT

At the time of design of the experiment a valued reference was a paper of Chang and Davis [1962] giving estimates of the distribution and absolute intensities of relativistic electrons in the magnetosphere of Jupiter that would yield the well-observed decimetric radio emission [Carr and Gulkis, 1969]. The most pertinent previous experience in observing such high intensities of relativistic electrons in space was that obtained following the 1962 high-altitude nuclear explosion (Starfish) in Earth's magnetosphere [O'Brien et al., 1962] [Van Allen et al., 1963] [Van Allen, 1966]. That experience served as a guide for instrument design. Other basic considerations in addition to the NASA constraints were simplicity, ruggedness, internal redundancy, large dynamic range, reliability over long flight periods, and insensitivity to radiation damage and temperature.

Seven miniature Geiger-Mueller tubes are used as basic detectors. Four of these (A, B, C, and G) are EON Corporation end-window type 6213 which have logged over 700,000 detector hours of reliable operation in University of Iowa instruments on a wide variety of earth-orbiting and planetary missions of long duration. Many individual tubes have logged over 10^{10} counts and a few, over 10^{11} counts. The three other tubes (D, E, F) are EON Corporation

type 5107 tubes, which had not been flown before but had proved, after stringent selection and testing, to have excellent reliability and a considerably lesser dead-time than do the 6213's. The seven tubes were placed in a variety of physical arrangements.

A, C, and B are mounted in a single block as shown in Figure 1. The central tube C is shielded omnidirectionally. A and B are similarly shielded except for thinner window, unidirectional collimators in the +X direction. The individual counting rates of the three tubes are telemetered separately; also double coincidences AB and triple coincidences ABC with a resolving time of 1 μs are formed and telemetered.

The second assembly comprises an omnidirectionally shielded, triangular array of three miniature, cylindrical tubes as shown in Figure 2. The rate of D and the triple coincidence rate DEF are telemetered.

The third assembly (Figure 3) uses a thin mica-window 6213 (1.3 mg/cm^2) (G) in scatter geometry with a gold-plated elbow as the entrance aperture. The purpose of the scatter arrangement is to admit low energy electrons (E_e > 0.060 MeV) but discriminate strongly against protons, E_p < 20 MeV.

The overall physical arrangement is sketched in Figure 4. The Z-axis of the instrument is parallel to the axis of rotation of the spacecraft. The +X axis points outward into free space from the rim of the instrument compartment of the spacecraft. The

magnetometer and a portion of the magnetometer-boom subtend a trivial fraction of the fields of view of the collimators of A, B, and C; otherwise there is no physical obstruction within the fields of view.

The instrument uses 12 bits (4 words) in each 192-bit main science frame (MSF) of the spacecraft's telemetry format (i.e., 6.25% of science telemetry) in science formats A or B. Quasi-logarithmic data compression is used to maintain 1% accuracy at all possible counting rates. All outputs are digital. A complete cycle of University of Iowa data comprises eleven MSF's as follows: Sync Word, G, A, B, G, AB, ABC, C, D, ABC, and DEF. Thus the individual accumulation duty cycles are 9.1% for A, B, C, D, AB, and DEF, and 18.2% for G and ABC.

Counts from each detector channel are accumulated for a period of time in seconds equal to 192/b, where b is the telemetry rate in bits/second for the entire spacecraft (b = 16, 32, 64, 128, 256, 512, 1024, or 2048, as selected by ground command).

During the Jovian encounter the prevailing value of b was 1024 bits/second and the telemetry format was mainly D/B with some segments in format B (as sketched above). In format D/B the duty cycles of our detectors are the same as in formats A or B but the sampling time is doubled. Hence, each data sample corresponded to an accumulation time of 0.375 second, or to a rotational angle of 10.7 at the prevailing spacecraft rotational period of 12.6

seconds. Successive samples from each channel are taken at intervals of 4.125 seconds or 118° of rotational angle. The rotational axis (+Z) of the spacecraft is pointed continuously at the earth with an error of less than 1° and therefore lies approximately in the ecliptic plane. Angular distributions of particle intensities as a function of roll angle in the equatorial plane of the spacecraft are assembled as a soft-ware operation using attitude data supplied by the Ames Research Center. In our analyses the roll angle is measured from the ascending node of the spacecraft's equator on the ecliptic to the +X-axis of the instrument (Figures 1, 2, 3, and 4) at the mid-time of the sample. It is noted that the Z-axis of the S/C is approximately orthogonal to the $\vec{B}$ vector of the planet during the central portion of the encounter. Hence a nearly complete scan of particle pitch angles is obtained. (This is not true in the outer portion of the planet's magnetosphere.) A useful angular distribution can be assembled for each detector channel for each minute and a nearly complete one for each 3.6 minutes of total observational time.

All data transmission during the encounter was in real-time except for a period of 64 minutes during which the spacecraft was occulted by the planet; during this period data were stored for 51.2 minutes at 16 bits/second in Format B in a 49,152 bit accumulator and subsequently played back.

Our instrument is designed to operate continuously throughout flight in a single mode as described above. Two completely redundant logic packages are provided internal to the instrument. Command switching from "main" to "standby" processor is the only mode change provided other than "power on", "power off" commands. No malfunctions of any kind in the University of Iowa instrument have been detected during some 26 months of continuous in-flight operation, including the Jovian encounter and the post-encounter period to date of writing. The instrument temperature during encounter was +4 °C, comfortably near the center of the range for proper operation -20 °C to +40 °C.

The total mass of the instrument is 1.64 kg and the total power required 0.76 watt.

PHYSICAL CALIBRATION OF THE DETECTORS

The original design of the instrument was done principally on a calculational basis. Following completion of the prototype and flight instruments an extensive series of physical calibrations (in addition to standard environmental qualification tests) was made with the following radiation sources:

(a)   Variety of β sources (C^{14}, Ni^{63}, Tc^{99}, Sr^{90}, Tl^{205})

                                (U. of Iowa)

(b)   5000 curie Co^{60} source of gamma rays

                                (U. of Iowa)

(c)   30-230 kV d.c. x-ray machine

                                (U. of Iowa)

(d)   0.3 - 1.8 MeV Van de Graaff accelerator for protons

                                (U. of Iowa)

(e)   1-6 MeV Van de Graaff accelerator for protons

                                (U. of Iowa)

(f) β-ray spectrometer ($\sim$50-600 keV)

                                (U. of Iowa)

(g)   Van de Graaff accelerator for electrons 0.2 - 1.6 MeV

                                (GSFC)

(h)   0-300 kV d.c. electron accelerator

                                (U. of Iowa)

(i)   Variable energy cyclotron for protons 15-100 MeV

(U. of Maryland)

(j)   Linac for electrons 5-40 MeV

(Argonne Cancer Research Hospital)

(k)   Linac for electrons 20-100 MeV

(Gulf Radiation Technology Laboratory, now Intelcom Rad Tech)

(ℓ)   Synchrocyclotron for protons ~ 100-570 MeV

(Space Radiation Effects Laboratory)

The full body of calibration data has been assembled and analyzed by Baker [1973]. A re-analysis and further digest of "unit response functions" for monoenergetic beams are summarized in Figure 5 for electrons and in Figure 6 for protons. It is noted that the ordinate in each case is in absolute units -- namely count/sec for an isotropic beam of monoenergetic particles having an omnidirectional intensity of one particle/cm^2 sec. Inasmuch as all calibrations were done with actual particle beams, effects of locally produced bremsstrahlung, etc. are automatically included in the response functions.

The only significant shortcomings of Figures 5 and 6 are the assumption of particle isotropy and the omission of the influence of the spacecraft, on the outer edge of which our instrument is mounted. For a continuously rotating spacecraft, the assumption of isotropy causes an error of the order of 25% or less for the types of angular distributions actually observed. This error can be

reduced by iteration, when worthwhile to do so. The spacecraft and its contents (mostly low Z-material) subtend an effective solid angle of about 30% of the unit sphere centered on the detectors. On the one hand, this mass of material acts as an absorber, thus tending to decrease counting rates. On the other hand, it acts as a generator of multiple particle events via bremsstrahlung, pair production, etc., thus tending to increase counting rates.

For protons E_p < 100 MeV and electrons E_e < 20 MeV, the absorption effect probably dominates; for electrons, E_e > 20 MeV, the production of secondaries probably dominates. Observed multiple coincidence rates during high energy electron tests in the laboratory and during the Jovian encounter are sufficiently low to suggest that the multiplicative effects in the spacecraft are not important. Lacking a thoroughly definitive test of this matter we have adopted Figures 5 and 6 without any correction for spacecraft influence. The overall uncertainty in the absolute intensities quoted hereafter is probably of the order of 50%.

Using the monoenergetic, unit response functions of Figures 5 and 6 we have subjected each detector, calculationally, to isotropic beams of electrons and protons (separately) having continuous power-law or exponential spectra with arbitrary differential spectral index γ or e-folding energy E_o, respectively.

The resulting absolute geometric factor (cm^2) is then a function of γ, or E_o, and of the assumed threshold energy. These calculations yield "bow-tie" diagrams such as those shown for electrons in Figure 7. The approximately coincident crossing-points of the several curves in each diagram enable one to assign a single pair of effective values of absolute geometric factor and threshold that are approximately independent of spectral form. Our adopted values are tabulated in Table 1.

The differences in counting rates (G-C), (B-C), and (A-C) are attributed to particles entering the collimators of G, B, and A, respectively, on the assumptions that the omnidirectional shielding of G, A, B, and C is identical and that the individual tubes are identical. During most of the Jovian encounter the ratios (G-C)/C, etc. are substantially greater than unity and inaccuracies in these assumptions produce no significant error. However, near periapsis the several ratios shrink to near unity and the formally inferred values of the intensities of electrons E_e < 21 MeV are subject to considerable uncertainty. Otherwise stated, the problem is one of differencing two large and somewhat uncertain counting rates and ascribing the difference to a collimator whose solid angle is a small fraction of 4π (Table 1). Appropriate qualifications are repeated at relevant points later in the paper.

A valuable overall validation of the detector calibrations was obtained from observations during traversal of Earth's outer

radiation belt and magnetosheath by Pioneer 10 on March 3, 1972
in the range $5.2 \leq L \leq 6.2$ and $8 < L < 29$ earth radii. Angular
distributions and absolute intensities of electrons $E_e > 60$ keV
and > 550 keV were in good agreement with well established values
[Van Allen, 1972].

The dynamic range of the individual GM tubes extends to at
least 10^7 counts/sec in the manner illustrated in Figure 8. Such
r vs R curves were run repeatedly and over a wide range of tempera-
ture (-20 °C to +25 °C) for each detector in the completed flight
unit using a d.c. x-ray machine and a 5000 curie Co^{60} source of
γ-rays. They were also checked at the maximum with protons and
electrons. The r vs R curves for all detectors are generally
similar though they differ among themselves in detailed shape.
Dependence on temperature has been virtually eliminated during
development of the associated electronics. As will be seen later,
the operating points of detectors A, B, C, and G (but not D)
moved up to and beyond the peaks of their r vs R curves during
traversal of the central part of the Jovian magnetosphere. Near
the peak of the curve, dr/dR is approximately zero and the apparent
(observed) rate is insensitive to changes in the true rate. To the
right of the peak, a reasonably accurate determination of R again
becomes possible. The basic ambiguity between the left and right
hand branches of the curve can be resolved by distinctively
different statistical fluctuations in the apparent counting rate

of an individual detector and by the general run of data from the several different detectors.

A specific problem in the near-periapsis data occurred. The maximum observed rates of A, B, C, and G were all significantly greater (by 1400-2100 counts/second) than those of the laboratory calibration curves. After eliminating a number of conceivable causes for this discrepancy, we have concluded that the most likely cause was slight upward drifts in the voltage of the gas-filled corona regulator tubes (Victoreen GV1A) which control the high voltage supplied to the GM tubes. The effect is simulated by changing the nominal 700 volts by 1-2%. The manufacturer advises us that aging drifts of this magnitude occur commonly in long-term bench tests of operating GV1A's.

After examination of data from the Jovian encounter (the only in-flight episode that has or probably ever will exercise the detectors to the peaks of their r vs R curves) we ran families of r vs R curves as a function of voltage for similar tubes. We then selected a member of the family that closely resembled the pre-flight curve for each detector and then the corresponding member at such a higher voltage as to exhibit the same peak value of r as observed on that detector during the encounter. The latter was then adopted as the basis for converting apparent rates to true rates. Figure 8 illustrates the adopted solution to the problem for detector G, a typical case.

No one of the individual GM tubes can distinguish electrons from protons. However, combinations of detectors have useful (and in some cases conclusive) diagnostic properties for determining the particle species that is dominantly responsible for a given set of observed counting rates. These methods rely on ratios and differences of individual counting rates and on multiple coincidence rates. One such ratio is DEF/D. Its laboratory value for electrons is shown in Figure 5, with a maximum of 2×10^{-2} at $E_e \approx 70$ MeV, whereas for protons $E_p < 150$ MeV it is less than 10^{-5} and for protons $150 < E_p < 500$ MeV it is $\leqslant 2 \times 10^{-3}$ (Figure 6). In the inner magnetosphere of Jupiter the observed ratio was $\approx 10^{-2}$, thus showing that the response of D was attributable primarily to electrons $E_e > 20$ MeV.

Another simple diagnostic relating to high energy particles is the ratio of the counting rates of C and D. C and D have essentially the same proton energy threshold but markedly different electron energy thresholds (Table 1). For a pure proton beam of any spectral form, $C/D \approx 2.8$. For electrons, C/D depends on the form of the spectrum and ranges from ≈ 3.4 for $\gamma_e = 1.5$ to ≈ 14.5 for $\gamma_e = 5.0$ (γ = differential spectral index). The values of C/D observed throughout the Jovian magnetosphere lie primarily in the range 4.0 - 7.0. These values correspond to electrons being the primary contributor to the counting rates of both C and D.

For lower energy particles, the ratio of the counting rates of detectors G and B provide the best species identification. By comparing the electron and proton response functions (Figures 5 and 6) of these two detectors one sees that G responds almost negligibly to protons $E_p < 20$ MeV. B, however, has a threshold of unidirectional response to protons of $E_p = 6.6$ MeV. For electrons, the order of the thresholds is reversed with G's threshold at $E_e \approx 0.040$ MeV and B's at $E_e \approx 0.20$ MeV. The effect of these relations is that G/B is markedly > 1 when the lower energy particles are predominantly electrons and is < 1 when protons dominate (and when $1.0 < \gamma_p \leqslant 1.5$). In all but isolated regions, throughout encounter, G/B > 1. Specifically for $r \leqslant 20$ R_J, G/B is $\geqslant 1.5$. Thus, lower energy protons contribute much less than do electrons to the counting rates of G and B in this region.

It appears that the responses of A, C, and D are caused dominantly by electrons at all times during the Jovian encounter. Within a radius of 20 R_J, the responses of G and B are also caused dominantly by electrons. During isolated segments of data in the outer magnetosphere, low energy protons contribute significantly to the responses of G and B.

Our internal identification analysis is consistent with data from other Pioneer 10 experiments [Simpson et al., 1974] [Trainor et al., 1974] [Fillius and McIlwain, 1974].

ENCOUNTER TRAJECTORY

In order to understand the run of observations, it is valuable to have at hand a general view of the encounter trajectory. One such diagram in planet-centered inertially oriented coordinates is Figure 9, a projection on the ecliptic plane of the hyperbolic trajectory of the spacecraft and of the orbits of the four inner satellites of Jupiter. The inclination of the planet's orbital plane to the ecliptic plane is $1°3$ and of its equatorial plane to its orbital plane is $3°1$. Also the orbital planes of the inner satellites are nearly coincident with the planet's equatorial plane. Hence the three basic reference planes are interchangeable for approximate purposes.

A second diagram of essential importance is one showing the time-trace of the spacecraft in magnetic polar coordinates. Any such trace is, of course, dependent on the assumed model of the external magnetic field of the planet. An example of such a diagram is Figure 10. The parameters of the model of the magnetic field as shown in Figure 10 arise from analysis of our particle data as described in a later section.

In order to maintain consistency within the Pioneer 10 project, the JPL/ARC value of 71,372 km has been adopted as

"the radius of Jupiter" ($= 1$ R_J). Geometric distances and values of the McIlwain L-parameter are expressed in terms of this unit. The above value is within 0.3% of the best current value of the planet's equatorial radius.

NOTE ON TIME-LABELING

Throughout this paper, we time-label observed data with the Greenwich Mean Time at which the data were received at the earth ("Earth Received Time" or ERT). Also, the position of the spacecraft is time-labeled with the ERT of the data that were being observed at the position so labeled. During the encounter, the time-of-flight of an electromagnetic signal from the spacecraft to the earth varied from 44.3 minutes at periapsis passage minus 10 days to 47.0 minutes at periapsis passage plus 10 days. A constant value of 46 minutes is of adequate accuracy for approximate purposes. For example, if one imagines that the spacecraft carries a Greenwich Mean Time clock which reads 0202 at a position P, this position is time-labeled 0248, as are the data observed at P.

NOTES ON COORDINATE SYSTEMS AND
KINDRED MATTERS

Three different, planet-centered, rotating coordinate
systems (I, II, and III) are in common use for specifying identifi-
able physical features of Jupiter. All measure latitude from the
equatorial plane. The three different longitudes are measured
from different meridians, but all increase westward, i.e., in the
sense opposite to the sense of rotation of the planet. Each of
the systems corresponds to a different period of rotation. Hence
the relationships among the three longitude values $(\lambda_I, \lambda_{II}, \lambda_{III})$
of a given object are time dependent; also the relationships are
a function of the distance of the object, if time at the object is
used. A sparse tabulation of System I and System II (but not
System III) longitudes of the central meridian of the planet as
viewed by a terrestrial observer (at particular values of ERT) is
given routinely in the annual American Ephemeris and Nautical
Almanac. Also given are accurate but sparse data on the ephemerides
of the satellites for the use of terrestrial observers   (See also
Explanatory Supplement to the Astronomical Ephemeris and Nautical
Almanac, 1961, and the Supplement to the A.E. 1968, 1966.)
[Peek, 1958] [Marth, 1896]. The Pioneer 10 trajectory as supplied

to experimenters by the Ames Research Center tabulates longitude of the spacecraft (at "spacecraft time") as the negative of λ_I according to the Jet Propulsion Laboratory convention [Melbourne et al., 1968]. A valuable digest of all of the above has been made by Mead [1973], who gives the following conversion formulae as applicable <u>at Jupiter</u> (or approximately to a nearby spacecraft):

$$\lambda_{III} \ (1957.0) \ = \ \lambda_{II} + 0.27432 \ (J - 2435839.5)$$

$$\lambda_{II} \ = \ \lambda_I - 7.63 \ (J - 2435839.5) - 70.78$$

$$\lambda_{III} \ (1957.0) \ = \ \lambda_I - 7.35568 \ (J - 2435839.5) - 70.78$$

where all longitudes are in degrees and J is the Julian date, at Jupiter.

The System III or "magnetospheric" longitude [I.A.U. Info. Bull. No. 8, 1962] is based on radio astronomical measurements and is the one presumably most relevant to the present investigation. We have converted the longitude of the spacecraft to System III (1957.0) using the above formulae.

Further, according to Mead's [1973] digest of radio astronomical data, the tilt of a centered dipole (representing the external magnetic field of the planet) is about $10°$ to the rotational axis and the System III (1957.0) longitude of its pole is about $224°$ as extrapolated to 1973.9.

Accurate ephemerides of the five inner satellites of Jupiter were kindly supplied to us by M. Helton of the Jet Propulsion Laboratory.

REVIEW OF ENCOUNTER OBSERVATIONS

The first durable encounter with the magnetosphere of
Jupiter occurred at 2024 ERT on November 26, 1973 (Figure 11).
At that time the radial distance of the spacecraft from the
center of the planet was 109 R_J (7.8 x 10^6 km) and its local
time was 9.7 hours. The counting rates of our lowest energy
threshold detectors G and B (cf. Table 1) began a clear and pro-
gressive increase above interplanetary rates. The causative
particles are primarily electrons E_e > 0.060 MeV. Also at that
time a weak but characteristic bow shock signature appeared in
data from both the magnetometer [Smith et al., 1974] and plasma
analyzer [Wolfe et al., 1974]. During the 24-hour period
1200/November 25 to 1200/November 26 the fluctuating inter-
planetary magnetic vector had an average cone angle of 116°
(polar angle from +Z-axis of spacecraft, which was earth-
pointed), an average clock angle (rotational angle measured from
the ascending mode of the spacecraft's equatorial plane on the
ecliptic plane to $\vec{B}$) of 18° (i.e., slightly northward-pointing
relative to the ecliptic), and an average magnitude of 0.67 γ
(gamma). Beginning at about 1200/November 26 the cone angle
changed discontinuously to $\approx$ 140°, the clock angle crept upwards

toward a value of $\approx 60°$, and the magnitude changed to an erratic but lower value of about 0.3 γ. This general region is labeled "pre-shock" in Figure 11. In the magnetosheath the magnetic vector was quite irregular in direction and magnitude with an average magnitude of 2 to 3 times its interplanetary value. At 2038/November 27 both magnetometer and plasma analyzer data identified a magnetopause signature. Also, the counting rates of our particle detectors (including the heavily shielded ones) began a distinctive and discontinuous increase, though less abruptly than did the magnitude of the magnetic vector.

After passage through the magnetopause (Figure 12) there were generally rising counting rates on all detectors. The most distinctive feature of this period was a regular periodic variation, more or less coherently on all detectors, with a period of about 10 hours. This period is identified with the planet's System III rotational period of 9.9249 hours [Carr, 1971]. The regular pattern of variability was interrupted by a 6-hour "drop-out" to interplanetary values in the counting rates of all channels during the period 0500 to 1100 on December 1. Thereafter, the generally upward trend of counting rates of all detectors resumed as though the drop-out had not occurred and the periodicity reappeared. However, for the first cycle following the drop-out, the counting rates of lower energy detectors G and B were out-of-phase with those of the higher energy detectors A, C, and D by about 180°.

This phase-shift disappeared and coherence was reestablished by midday of December 2.

Beginning at about 0800/December 3 ($r = 19$ R_J), all counting rates began a strong upward climb of several orders of magnitude (Figure 13) and reached their greatest values at 0215/December 4, about an hour before periapsis passage at 0315 at $r = 2.84$ R_J. The rates then declined to a deep minimum at 1545 ($r = 13.4$ R_J).

Thereafter the periodic, coherent variation of counting rates resumed, with broader minima and flatter maxima than on the inbound leg of the trajectory, and with generally declining values (Figure 14). This pattern persisted until late on December 9 ($r \approx 88$ R_J). Then for about a day, the pattern of variability more nearly resembled that of the inbound leg of the trajectory. At about 1300/December 10 ($r = 98$ R_J) an abrupt, coherent cut-off in all counting rates occurred and they all dropped to interplanetary values. However, sporadic activity resumed (Figure 15) about 20 hours later and persisted through at least December 16 ($r = 170$ R_J). Isolated bursts of particles, presumably from Jupiter, continued to occur for many days thereafter.

THE MAGNETODISC

The pervasive 10-hr periodicity (or modulation) in the counting rates of all detectors in the outer magnetosphere of the planet on both the sunward (inbound) and dawn (outbound) sides is identified with the rotational period of the planet. The System III (sidereal) rotational period derived from radio (e.g., magneto-spheric) emissions (both decametric and decimetric) is 9 hr 55 min 29.75 ± 04 sec = 9.9249 hr [Carr, 1971].

We consider that our particle observations taken together with the magnetic field observations [Smith et al., 1974] and rudimentary theoretical considerations make it virtually conclusive that the outer magnetosphere of Jupiter has the physical shape of an immense, relatively-thin disc. We have adopted a suggestion by William Dixon that this portion of the Jovian magnetosphere be referred to as the magnetodisc.

In our earlier paper [Van Allen et al., 1974a], we showed that a thin, tilted, rigid disc attached to the planet and having, as observed, a radially distended magnetic field and an accompany-ing population of confined, or quasi-trapped, energetic particles gives a good first order representation of the observations. It was further supposed that the basic cause of the distention of the

field is thermal plasma (not directly observed) corotating with the planet and subject to an approximate balance of forces -- gravitational, pressure gradient, magnetic, and centrifugal. It is of interest to note that at 100 R_J the circumferential velocity of a corotating parcel of plasma is 1250 km/sec, over three times as great as a typical solar wind velocity.

Indirect evidence for the presence of thermal plasma is provided by the approximate "nulls" and strong fluctuations in direction of the magnetic vector $\vec{B}$ that occur at or near the centers of our charged particle peaks. This phenomenon is especially clear on the outbound leg of the trajectory (dawn side). One of the best of many examples is shown in Figure 16.

Some authors have argued that the magnetodisc is comprised of outward streaming particles. Although it is difficult to exclude this possibility completely, we continue to favor the view that the energetic particle population in the magnetodisc is quasi-trapped, though no clear basis for estimating residence times has yet occurred to us. A variety of evidence having various levels of persuasiveness is as follows:

(a) The magnetodisc is thin in its axial dimension ($\leqslant$ 10 R_J) and has sharp boundaries (≈ 1 R_J). Such sharpness is compatible with magnetic confinement of electrons of the energies observed. For example, electrons of E_e = 0.1, 1.0, and 10 MeV have gyro-radii in a 5γ magnetic field of 0.003, 0.013, and 0.098 R_J, respectively.

(b) Our angular distribution studies exclude unidirectional streaming along magnetic field lines. Indeed the predominant form of angular distribution in the magnetodisc is approximate isotropy with noteworthy exceptions in which the distribution has pronounced and equal maxima along both $+\vec{B}$ and $-\vec{B}$ ("dumbbell" distribution) or orthogonal to $\vec{B}$ ("pancake" distribution), clearly requiring quasi-trapping for times long compared to a latitudinal bounce period.

(c) The persistent 10-hr periodicity out to ≈ 100 R_J suggests closed rather than open magnetic field lines in order that the diurnal wobbling of the dipole be transmitted to the point of observation.

(d) An approximate integral of the magnetic flux through the magnetodisc outside of 20 R_J (magnetic latitude $\approx 77°$) suggests that there is little or no "polar cap" of open, unpopulated field lines.

(e) The particle intensities decline, in general, with increasing radial distance. This fact might be consistent with either outward streaming or quasi-trapping but the outer boundary is relatively sharply defined (Figures 12, 14, and 15), thus favoring confinement.

(f) Approximate axial symmetry of particle populations in the magnetodisc over some five hours of local time suggests residence times comparable to or greater than a rotational period (10 hr).

It should be noted (Figure 9) that the angle between the magnetic vector (approximately radial) and the spin axis of the spacecraft is markedly different on inbound and outbound legs of the trajectory in the outer magnetosphere. On the inbound leg our low energy detectors make only a partial scan of particle pitch angles relative to local magnetic vector, almost never reaching pitch angles near 0° or 180°, whereas relatively complete scans of pitch angles are usual on the outbound leg. This fact may account, in part, for the difference in the modulation pattern of counting rates on the inbound and outbound legs of the trajectory, as is evident by comparing Figure 12 with Figure 14. Another, and perhaps more significant, reason is suggested by noting that the modulation pattern on the outbound leg from 2100/December 9 to 1300/December 10 (Figure 14) and from 0000/December 13 to 2000/December 14 closely resembles that of the inbound leg. Both of these periods occurred before magnetopause crossings. Hence, buffeting by the solar wind on the sunward side of the magnetodisc and on its outer fringe on the dawn side may tend to destroy the well ordered geometric form that it has at lesser radii on the dawn side. Such a line of thought is also compatible with the disorderly and more orderly nature of the magnetic field in the respective regions.

One feature of special interest is the drop-out of particle intensities on December 1. The plasma analyzer experimenters

[Wolfe et al., 1974] suggest that this is caused by a dramatic
inward movement of the sunward magnetopause, caused by an impulsive
increase in solar wind pressure. For the sake of discussion, we
adopt a competing view, namely that a plasma instability developed
in the outer magnetodisc, that field line interconnection occurred
at $\approx$ 50 R_J, and that a "bubble" of magnetized plasma "spun off"
into interplanetary space, carrying a quasi-trapped population of
energetic particles with it [Gold, 1964 [Dungey, 1958]. Support-
ing evidence for this view is provided by the subsequent observa-
tion of a passing bubble of energetic particles by our instruments
on Pioneer 11 (Figure 17), which was nearly along the same radial
line from the sun as was Jupiter and at a distance of 2.1 A.U.
closer to the sun. The apparent group velocity of this bubble
based on time between drop-out and passage of maximum intensity
is 1,140 km/sec, a value similar to the circumferential
velocity of the outer edge of the magnetodisc. The time profile
of the event is quite different than those of solar energetic
particle (SEP) events for similar particle energies and is in
fact similar to other Jovian energetic particle (JEP) events
observed as "precursors" and "post-cursors" by other Pioneer 10
experimenters [Simpson et al., 1974] [Trainor et al., 1974] and
confirmed by us.

One is reminded of the body of pulsar evidence on the time
variability of dispersion measure (the columnar integral of electron

density between pulsar and Earth) which is most plausibly attributed to spin-off of plasma from the rotating pulsar [Rankin and Roberts, 1971] [Rankin and Counselman, 1973]. Indeed, there appears to be a certain descriptive validity in thinking of Jupiter as a pulsar-like object, though the relevant physical parameters are of enormously different magnitude in the respective cases.

The existence of "switching anisotropies" (rapid transitions from unidirectional streaming in one direction to uni-directional streaming in the opposite direction) in the magnetodisc early on December 6 has been reported by Simpson et al. [1974]. We have examined our data for the same period at the same time resolution and confirm the rapid fluctuations and strong anisotropies. However, we find the angular distributions to be bi-directional (dumbbell) in form and not unidirectional thus contradicting their interpretation of close-by local acceleration.

The most common angular distribution of particle intensity in the magnetodisc ($r > 25 \, R_J$) is one of approximate isotropy. Significant exceptions occur as illustrated by four examples in Figure 18. Soon after the inbound crossing of the magnetopause on November 27 a weak but persistent pancake distribution appeared (upper left, Figure 18). At about 0500/November 28 this distribution changed over to one of dumbbell form and remained so (lower left, Figure 18) until 0600/November 29, after which time it became isotropic. Significant departure from isotropy was

observed again late on December 1 and early on December 2 (upper

right, Figure 18) following the drop-out early on December 1

(Figure 12). The distribution was of pancake form at that time;

by 0400/December 2, it had changed to dumbbell form, then moved

slowly to isotropy. The signature of the angular distribution

history during this epoch resembles that following the first

crossing of the magnetopause and thus tends to confirm the magneto-

pause-like character of the recovery from the drop-out in mid-day

of December 1. Such evidence does not distinguish between the

competitive hypotheses of impulsive spin-off or impulsive compres-

sion of the outer portion of the magnetodisc on December 1. A

transition from pancake to dumbbell form occurred in less than one

hour at about 1700/December 2, near a crossing of the magnetic

equator.

On the outbound leg, nearly isotropic distributions

predominate. Noteworthy exceptions occur, particularly on

December 6, when strong dumbbell distributions appear. An example

is given in the lower right panel of Figure 18.

No periods of unidirectional streaming have been identified

during either inbound or outbound traversals of the magnetodisc.

A detailed study of the periodic fluctuations in counting

rates in the magnetodisc has yielded significant modifications to

the first-order rigid disc model proposed earlier [Van Allen et al.,

[1974a] and has suggested some illuminating implications. The times

of minima in detector C on the inbound leg of the trajectory and of maxima in detector G on the outbound leg have been measured carefully on large scale working plots (of the nature of Figures 12, 14, and 15). These two different detectors were selected as giving the best definition on the respective legs of the trajectory. The System III longitude of the spacecraft (λ_{III}) at those times is plotted as a function of radial distance in Figure 19. If the disc were rigid with its pole at $\lambda_{III} = 224°$ all points would lie along the line labeled $44°$. It is seen that this expectation is, in fact, fulfilled out to $r \approx 25$ R_J. Beyond this radial distance the inbound and outbound curves curl markedly away from the rigid-disc line and in opposite senses. This effect is presumed to be one of local time. The inbound points (pre-noon) lead the line and the outbound points (pre-dawn) lag the line. The effect is interpreted in more detail by Goertz et al. [1974] in an accompanying paper as resulting from a composite of disc-flapping by the mechanism of transverse Alfvén waves and of local-time-and-latitude-dependent slipping of the feet of magnetic field lines in the ionosphere of the planet. The latter feature of the interpretation yields provisional estimates of ionospheric electric fields at high latitudes.

THE INNER MAGNETOSPHERE

Our discussion of the inner magnetosphere ($r \leqslant 20$ R_J) of Jupiter centers around the observations presented in Figure 13. Of companion importance are the magnetic field observations [Smith et al., 1974]. The regular dipolar magnetic field at radial distances $r \leqslant 10$ R_J undergoes a progressive transition to a markedly distended and often irregular form in the magnetodisc within about the same range of radial distance as that within which the distributions of energetic particles undergo a qualitative change in character.

The curves of Figure 13 give absolute omnidirectional intensities of electrons whose energy exceeds five different energy thresholds as shown (cf. Table 1). The bases for going from raw counting rate data to these curves have been discussed in detail in the section entitled Physical Calibration of Detectors. Briefly, the procedure is as follows:

(a) Each individual counting rate sample from each detector is corrected for dead-time using the appropriate, renormalized r vs R curve (as Figure 8, for example). Either the rising or falling branch of the curve is used as decided from a careful, earlier examination of the uncorrected data. This decision is an individualized one for each different detector.

(b) The corrected ("true") counting rates for the omni-directionally shielded detectors C and D are corrected to absolute intensities by the summary data of Table 1.

(c) For the directional detectors G, B, and A, the three differences of corrected, rotationally averaged counting rates (G-C), (B-C), and (A-C) are found for each interval of time. Each of these differences is assumed to correspond to a proper average over the unit sphere of the unidirectional intensity in the appro-priate energy range. The quantities (G-C), (B-C), and (A-C) are then converted to absolute omnidirectional intensities by means of Table 1, the factor 4π having already been incorporated into the listed values of reciprocal geometric factor.

(d) Finally, the respective intensity values from step (c) for $0.060 < E_e < 21$ MeV, $0.55 < E_e < 21$ MeV, and $5.0 < E < 21$ MeV are added to those of detector C ($E_e > 21$ MeV) as obtained in step (b). The three resulting curves as shown in Figure 13 are labeled $E_e > 0.060$, > 0.55, and > 5.0 MeV, respectively.

Solid lines in Figure 13 represent data that we consider worthy of a high level of confidence.

Dashed portions of the three upper curves are uncertain on the grounds discussed at length in the section entitled Physical Calibration of the Detectors. Further work is being done on this portion of the data to reduce uncertainties in effective omni-directional shielding and in dead-time corrections. Nonetheless,

the dashed portions of the three upper curves represent our best efforts to date and deserve provisional consideration.

The principal features of Figure 13 are as follows:

(a) All intensities tend generally upward to maximum values at about an hour before periapsis passage, then decline. The position of maximum intensities and the absence of symmetry in the curves are considered to be understood in terms of the nature of the trajectory in magnetic coordinates (Figure 10), as will be shown later.

(b) Detailed features in the curves (especially the upper three) appear to be plausibly associated with traversal of magnetic shells swept through by the three inner Galilean satellites (Figure 10).

(c) The two lowest energy channels show marked breaks in their upward climbs and a great deal of detailed structure in the vicinity of the inbound, near-equatorial crossing of the orbit of Ganymede. On the outbound, high-latitude crossing, there is a large and rapid decline in intensities of electrons of all energies. Only a small fraction of this decline can be attributed to "normal" latitude dependence of intensity (see later).

(d) There are clear and unequivocal notches in the upper two curves and a local plateau in the next lower curve at the inbound crossing of the orbit of Europa, at relatively high magnetic latitude. On the outbound crossing (nearer the

magnetic equator) there are clear plateaus and considerable structure in the upper three curves.

(e) At both inbound and outbound crossings of the orbit of Io there are similar notches in the upper three curves. These two crossings are at similar magnetic latitudes.

(f) Satellite effects in the lower two, higher energy curves are weak or indiscernible, except for the marked Ganymede dip on the outbound traversal of its magnetic shell.

(g) Although not shown in Figure 13, we have found no effects associated with either crossing of the orbit of Callisto, probably because its orbit ($r = 26.38$ R_J) lies outside of the well-ordered magnetic field of the planet.

(h) In a later paragraph it is suggested that Amalthea, whose orbit (of radius 2.54 R_J) is slightly interior to the periapsis of Pioneer 10, may have a significant sweeping effect on the population of energetic particles.

Our measurements of particle intensities can yield, at best, only a crude estimate of the magnitude of the magnetic moment of the planet. On this point, the direct magnetometer measurements are far superior. However, the particle measurements provide an independent and perhaps superior determination of the orientation of the axis of the moment. For an initial treatment we have concentrated on the use of the data from detectors C and D.

The procedure is an attempt to find, by trial-and-error, values of the tilt and System III longitude of the pole of a centered dipole such that the inbound and outbound intensity data are coincident when plotted as a function of the magnetic shell parameter L. The further, essential parameter is the form of the pitch angle distribution of unidirectional intensity at the magnetic equator, which may be a function of L. This process of three parameter minimization of inbound vs. outbound residuals has not yet been carried out in a sophisticated way. But the results of a rough minimization are considered quite illuminating and worthy of being reported at this stage.

The process is illustrated by a series of plots. A preliminary analysis [Van Allen et al., 1974a] showed that the angular distribution of intensity in the inner magnetosphere is of pancake form. For analytical convenience we have adopted the form

$$j\,(\alpha) \propto \sin^m \alpha$$

wherein j represents the unidirectional intensity and α the local pitch angle. In a quasi-time-stationary trapping situation, this angular distribution, if true at the magnetic equator for particles of a given species and energy, is true at every other point on the same L-shell for the same class of particles. Also the omnidirectional intensity J varies with the ratio of the magnitude of

the local magnetic field B to its magnitude at the equator B_o as
follows:

$$\frac{J(B)}{J(B_o)} = \left(\frac{B_o}{B} \right)^{m/2} .$$

For a dipolar magnetic field

$$\frac{J(B)}{J(B_o)} = \left(\frac{\cos^6 \Lambda}{\sqrt{4 - 3 \cos^2 \Lambda}} \right)^{m/2}$$

or

$$\frac{J(\Lambda)}{J(o)} = \left(\frac{\cos^6 \Lambda}{\sqrt{4 - 3 \cos^2 \Lambda}} \right)^{m/2}$$

wherein Λ is the magnetic latitude.

The first step in the process is shown in Figure 20. Here
we assumed the Smith et al. [1974] displaced dipole model and
sought the best value of m independent of L. The model was
relatively unsuccessful for any value of m, though $m = 4$ produced
about the best results.

We then tried centered dipoles with arbitrary values of
tilt, longitude of pole, and values of m. For m independent of L,
this search yielded a tilt of 9.5°, λ_{III} of the pole = 230°, and
m = 4 as a set of parameters that produced excellent closure in

the range $4.3 < L < 11$ R_J (Figure 21). We have found it impossible
to produce closure for $L > 11$ R_J with any dipolar model.

Examination of families of diagrams such as Figure 10
suggested that the open loop for $L < 4.3$ R_J might simply be a
manifestation of a rapid monotonic increase of m as L diminishes.
Figure 22 shows the results of adopting a simple dependence of m
on L, keeping the tilt and longitude of the pole as before. This
figure represents our most successful effort thus far on
detector C, for electrons $E_e > 21$ MeV. A similar effort on data
from detector D for electrons $E_e > 31$ MeV yields Figure 23.

Thus for both energy ranges, we achieved excellent closure
of inbound and outbound data in the range $2.9 < L < 12$ with a
centered dipole having tilt of $9.5°$ to the rotational axis of the
planet and with its pole at λ_{III} (1957.0) = $230°$. Changes of
these values by more than ± 0.5 or $\pm 3°$, respectively, produce
a discernible deterioration in closure.

For C: $m = 3.5 + (3.86/L)^8$

For D: $m = 4.0 + (3.567/L)^8$

Both of these empirical formula are for $L > 2.9$ R_J. There is no
assurance that they are valid for lesser values of L.

By least squares fitting to the data of Figures 22 and 23
in the range $3.5 < L < 12$ R_J and use of Table 1, we find

$$J \, (E_e > 21 \text{ MeV}) \;=\; 3.0 \times 10^8 \, \exp \, (-L/1.45) \left(\frac{\cos^6 \Lambda}{\sqrt{4 - 3 \, \cos^2 \Lambda}} \right)^{m/2}$$

and

$$J \, (E_e > 31 \text{ MeV}) \;=\; 9.9 \times 10^7 \, \exp \, (-L/1.51) \left(\frac{\cos^6 \Lambda}{\sqrt{4 - 3 \, \cos^2 \Lambda}} \right)^{m/2}$$

with J the omnidirectional intensity in absolute units electrons/cm^2 sec, L in units of R_J, and Λ the magnetic latitude in the dipolar model previously described. The values of m are given in an immediately preceding paragraph for C and D, respectively.

It is tempting to attribute the roll-over of both curves at low L values to a sweeping effect of Amalthea. A diffusional analysis will be useful in assessing the validity of this suggestion. Also, the follow-on mission Pioneer 11 is now targeted for a periapsis of 1.6 R_J. Its data should contribute to knowledge of this matter.

For L > 12 R_J is appears hopeless to match inbound and outbound data with any magnetic source entirely interior to the planet. The general failure to accomplish closure is presumably attributable to a system of external magnetospheric currents, such as those so obviously necessary to account for the magnetodisc. A special feature of the lack of closure is the great notch in the outbound pass in the vicinity of L = 15 R_J (Figures 22 and 23). By

reference to Figure 10, it is noted that the inbound traversal of this magnetic shell is near the equator whereas the outbound pass is at a latitude of about 22°. We attribute this notch to Ganymede. The value of m required to produce closure in this region is about 12. Such a thin pancake distribution is qualitatively compatible with the expectations of inward diffusion of particles past a satellite [Mead and Hess, 1973] [Birmingham et al., 1974]. A comparable, though less pronounced, effect at the two crossings of the orbit of Europa has been noted earlier in the low energy but not the high energy channels.

During most of the traversal of the magnetodisc and the inner magnetosphere there is no simple power law or exponential spectrum in energy that gives a good representation of the data over the full energy range provided by our five basic detectors. We have adopted a two-part power law fit

$$\frac{dJ}{dE} \propto E_e^{-\gamma_1}$$

in the energy range $0.06 < E_e < 5$ MeV and

$$\frac{dJ}{dE} \propto E_e^{-\gamma_2}$$

in the energy range $E_e > 5$ MeV.

In the magnetodisc, typical values are $1.6 < \gamma_1 < 2.0$ and $3.0 < \gamma_2 < 4.5$.

In the region $2.9 < L < 7.0 \ R_J$, values of γ_2 as inferred from C/D ratios are shown in Figure 24.

In the region $8 < L < 18 \ R_J$, provisional values of both γ_1 and γ_2 are plotted in Figure 25.

REMARKS

A retrospective assessment of the nature of the Pioneer 10 encounter trajectory confirms the wisdom of its choice for a first reconaissance. But, as with any single planetary fly-by, there are obv. ous deficiencies in coverage. From the standpoint of magnetospheric physics, there is a clear need for (a) observations at lesser radial distances (from which most of the decimetric radio noise emission occurs), (b) a survey of the inner magnetosphere at higher latitudes, (c) observations on the evening side of the planet at large radial distances, and (d) observations on the anti-solar side of the planet at radial distances of hundreds of planetary radii to search for magnetotail phenomena.

The targeting of the follow-on mission Pioneer 11 (periapsis passage on 3 December 1974) is designed to remedy several of these deficiencies as well as to provide a subsequent fly-by of Saturn. Also Pioneer 11 carries a considerably improved version of our experiment.

In March-April 1976, Pioneer 10 will cross the radial line from the sun through Jupiter. A search for magnetotail phenomena will be made at that time, though the Jupiter-spacecraft distance will then be 4.7 A.U. (astronomical units) or 9900 R_J.

If it is assumed that the magnetodisc of Jupiter extends to as great a distance on the dusk side as it has been observed to do on the dawn side, then its diameter perpendicular to the sun-planet line is at least 2.4×10^7 km. Such a distance subtends $2\overset{\circ}{.}3$ as Jupiter is viewed from the earth at opposition.

In addition to its overall intrinsic interest, the magnetosphere of Jupiter offers the following features which are distinctively different than that of Earth:

(a) Because of the great value of Jupiter's magnetic moment 1.45×10^{30} gauss cm^3 [Smith et al., 1974] or 1.8×10^4 times that of Earth, the physical scale of the Jovian magnetosphere is very much greater. By the same token the intensities and characteristic energies of inward-diffusing electrically-charged particles are also much greater.

(b) At the same planetocentric distance as measured in the respective planetary radii the centrifugal force on a parcel of plasma in the equatorial plane of Jupiter is 65 times as great as that at Earth. For this reason, the great magnetodisc of Jupiter has no terrestrial counterpart; rather it gives Jupiter a certain physical resemblance to a pulsar.

(c) The spin-off of plasma and energetic particles from the outer magnetodisc is a new planetary phenomenon (at least quantitatively). It provides an important new tool for investigation of the interplanetary propagation of energetic particles in the outer solar system, free of the complexities of the solar environment.

(d) The Moon's orbit lies outside of the central magneto-
sphere of Earth.   No discernible effect of the Moon thereon has
ever been shown to exist.   In contrast, the four inner satellites
of Jupiter produce massive sweeping effects on trapped particle
populations especially in the lower energy ranges as demonstrated
herein.   A more refined study of these effects promises significant
numerical results on both L-shell and pitch angle diffusion coeffi-
cients and hence on the basic dynamics of the magnetosphere.

In a companion paper Northrop and Birmingham [1974] have
calculated the decimetric radiation implied by our observational
data on energetic electrons.

The detail in our low energy electron data is inadequate
to assess the proposal of Gurnett and collaborators [Gurnett,
1972] [Hubbard et al., 1974] that the Jovian satellites act as
sources of energetic particles.

ACKNOWLEDGEMENTS

Table 1. Adopted Energy Thresholds and Geometric Factors for Pioneer 10 Detectors

Electrons[*]

Detector	Effective Energy Range	Effective Inverse Omnidirectional Geometric Factors (1/Q)	
G - C	0.06 MeV $< E_e < 21$ MeV	2600 cm^{-2}	Primarily
B - C	0.55 MeV $< E_e < 21$ MeV	830	Directional
A-C	5 MeV $< E_e < 21$ MeV	600	Detectors
C	$E_e > 21$ MeV	23.0	
D	$E_e > 31$ MeV	63.0	Omnidirectional

[*]Approximately valid for electron spectra with power law spectral indices $1.5 \leqslant \gamma_e \leqslant 4.0$.

Protons

Detector	Effective Energy Range	Effective Inverse Omnidirectional Geometric Factors (1/Q)
B - C	6.6 MeV $\leqslant E_p \leqslant 77.5$ MeV	620 cm^{-2}
A - C	30 MeV $\leqslant E_p \leqslant 77.5$ MeV	675
C	$E_p > 77.5$ MeV	8.2
D	$E_p > 77.5$ MeV	23.0

G - C   For $\gamma_p \leqslant 3.5$, protons of energy $E_p \leqslant 25$ MeV make a negligible contribution. For such a spectrum (G - C) is sensitive for $25 \leqslant E_p \leqslant 77.5$ MeV with $1/Q \approx 125$ cm^{-2}.

REFERENCES

American Ephemeris and Nautical Almanac, Annual Editions,

   U. S. Government Printing Office, Washington, D. C.

Baker, D. N., Calibration of University of Iowa instruments aboard

   Pioneers F and G, M.S. Thesis, University of Iowa, May 1973.

Birmingham, T., W. Hess, T. Northrop, R. Baxter, and M. Lojki,

   The electron diffusion coefficient in Jupiter's magnetosphere,

   J. Geophys. Res., 1974 (in press).

Carr, T. D., Jupiter's magnetospheric rotation period, Astrophysical

   Letters, 7, 157-162, 1971

Carr, T. D., and S. Gulkis, The magnetosphere of Jupiter, Annual

   Review of Astronomy and Astrophysics, 7, 577-618, 1969.

Chang, D. B., and L. Davis, Jr., Synchrotron radiation as the source

   of Jupiter's polarized decimetric radiation, Astrophys. J.,

   136, 567-581, 1962.

Dungey, J. W., Cosmic Electrodynamics, University Press, Cambridge,

   England, 1958.

Explanatory Supplement to the Astronomical Ephemeris and the

   American Ephemeris and Nautical Almanac, Her Majesty's

   Stationery Office, London, 1961.

Fillius, R. W., and C. E. McIlwain, Radiation belts of Jupiter,

   Science, 183, 314-315, 1974.

Goertz, C. K., T. G. Northrop, and M. F. Thomsen, The magnetosphere of Jupiter as observed with Pioneer 10. Part II: Non-rigid rotation of the magnetodisc, J. Geophys. Res., 1974 (accompanying paper).

Gold, T., Fields and particles in interplanetary space, Proc. International School of Physics - Enrico Fermi, Space Exploration and the Solar System, Course XXIV, Ed. Bruno Rossi, Academic Press, New York, 1964.

Gurnett, D. A., Sheath effects and related charged-particle acceleration by Jupiter's satellite Io, Astrophys. J., 175, 525, 1972.

Hubbard, R. F., S. D. Shawhan, and G. Joyce, Io as an emitter of 100-keV electrons, J. Geophys. Res., 79, 920-928, 1974.

International Astronomical Union, Information Bulletin No. 8, March 1962.

Marth, A., Ephemeris for physical observations of Jupiter 1896-97, Monthly Notices of the Royal Astronomical Society, 56, 516-534, 1896.

Mead, G. D., Magnetic coordinates for the Pioneer 10 Jupiter flyby, Unpublished Memorandum, Goddard Space Flight Center, April 1973.

Mead, G. D., and W. N. Hess, Jupiter's radiation belts and the sweeping effect of its satellites, J. Geophys. Res., 78, 2793-2811, 1973.

Melbourne, W. G., J. D. Mulholland, W. L. Sjogren, and F. M. Sturms, Jr., Constants and related information for astro-dynamic calculations, 1968, TR 32-1306, Jet Propulsion Laboratory, Pasadena, California, July 15, 1968.

Northrop, T. G., and T. J. Birmingham, The magnetosphere of Jupiter as observed with Pioneer 10. Part III: Jovian synchrotron radiation at 10.4 cm as deduced from observed electron fluxes, J. Geophys. Res., 1974 (accompanying paper).

O'Brien, B. J., C. D. Laughlin, and J. A. Van Allen, Geomagnetically trapped radiation produced by a high-altitude nuclear explosion on July 9, 1962, Nature, 195, 939-943, 1962.

Peek, B. M., The Planet Jupiter, Faber and Faber, London, 1958.

Rankin, J. M., and C. C. Counselman III, Pulsar NP 0532: variability of dispersion and scattering, Astrophys. J., 181, 875-889, 1973.

Rankin, J. M., and J. A. Roberts, Time variability of the dispersion of the Crab Nebula pulsar, Inter. Astron. Union Symposium No. 46, The Crab Nebula, D. Reidel Publishing Company, Dordrecht, Holland, 1971.

Simpson, J. A., D. Hamilton, G. Lentz, R. B. McKibben, A. Magro-Campero, M. Perkins, K. R. Pyle, A. J. Tuzzolino, and J. J. O'Gallagher, Protons and electrons in Jupiter's magnetic field: results from the University of Chicago experiment on Pioneer 10, Science, 183, 306-309, 1974.

Smith, E. J., L. Davis, Jr., D. E. Jones, D. S. Colburn, P. J.
Coleman, Jr., P. Dyal, and C. P. Sonett, Magnetic field of
Jupiter and its interaction with the solar wind, Science,
183, 305-306, 1974.

Supplement to the A.E. 1968, U. S. Naval Observatory, Washington,
D. C., 1966.

Trainor, J. H., B. J. Teegarden, D. E. Stilwell, F. B. McDonald,
E. C. Roelof, and W. R. Webber, Energetic particle population
in the Jovian magnetosphere: a preliminary note, Science,
183, 311-313, 1974.

Van Allen, J. A., Spatial distribution and time decay of the inten-
sities of geomagnetically trapped electrons from the high
altitude nuclear burst of July 1962, pp. 575-592 of
Radiation Trapped in the Earth's Magnetic Field, D. Reidel
Pub. Co., Dordrecht, Holland, Ed. B. M. McCormac, 1966.

Van Allen, J. A., Initial flight report on University of Iowa
experiment on Pioneer 10, University of Iowa Research Report
72-5, March 27, 1972.

Van Allen, J. A., L. A. Frank, and B. J. O'Brien, Satellite observa-
tions of the artificial radiation belt of July 1962,
J. Geophys. Res., 68, 619-627, 1963.

Van Allen, J. A., D. N. Baker, B. A. Randall, M. F. Thomsen, D. D.
Sentman, and H. R. Flindt, Energetic electrons in the magneto-
sphere of Jupiter, Science, 183, 309-311, 1974a.

Van Allen, J. A., D. N. Baker, B. A. Randall, and D. D. Sentman,
In situ observation of energetic particles in the magneto-
sphere of Jupiter, EOS, Trans. Am. Geophys. Union, 55, 336,
1974b (Abstract).

Wolfe, J. H., H. R. Collard, J. D. Mihalov, and D. S. Intriligator,
Preliminary Pioneer 10 encounter results from the Ames
Research Center plasma analyzer experiment, Science, 183,
303-305, 1974.

CAPTIONS FOR FIGURES

Figure 1.   Cut-away view of one system of detectors. A, C, and

B are miniature, end-window EON 6213 Geiger-Mueller tubes.

The Z-axis is parallel to the rotational axis of the space-

craft.

Figure 2.   Cross-sectional view of the heavily shielded triangular

array of miniature, cylindrical EON 5107 Geiger-Mueller

tubes D, E, and F.

Figure 3.   Cut-away view of the arrangement of the single EON

6213 Geiger-Mueller tube G. Low energy particles enter

the end-window of the tube only after being scattered from

the inner walls of the gold-plated elbow.

Figure 4.   Sketch of the overall configuration of the University of

Iowa instrument.

Figure 5.   Unit response functions of the several detectors for

monoenergetic electrons. See text for identity of the

accelerators used in determining these curves and for other

details.

Figure 6.   Unit response functions of the several detectors for

monoenergetic protons.

Figure 7. "Bow-tie" diagrams used in determining effective
energy thresholds and geometric factors approximately
independent of spectra form.

Figure 8. A sample pair of r vs R characteristic curves for
detector G. The solid curve to the left of $R = 10^5$
counts/sec and the dashed curve to the right of that point
represent the pre-flight calibration. The solid curve to
the right of $R = 10^5$ counts/sec is the renormalization of
this portion of the curve to the peak counting rate observed
during Jovian encounter.

Figure 9. Projection on the ecliptic plane of the hyperbolic
encounter trajectory of Pioneer 10 and the orbits of the
four inner Jovian satellites. The numbers 1 and 2 on the
orbits of JI, JII, and JIII show the positions of each
of these satellites at the time that the spacecraft crossed
the L-shell of that satellite, inbound and outbound
respectively. The number 3 shows the position of JV at
the time that the spacecraft was at periapsis, marked P.
$\gamma_{2\!\!\!\!\downarrow}$ designates Jupiter's vernal equinox and $\gamma_{\oplus}$ designates
Earth's vernal equinox. The ephemerides are courtesy of
M. Helton of the Jet Propulsion Laboratory. Note that the
spacecraft spin axis is parallel to the planet-earth line
throughout the encounter.

Figure 10. The time-labeled trace of Pioneer 10 in magnetic polar

coordinates (magnetic meridian plane projection) for the

planetary dipolar model as specified. The cross-hatching

shows the regions that bound the orbits of Io (JI),

Europa (JII), and Ganymede (JIII), respectively, in such

a coordinate system.

Figure 11. Detailed magnetic field strength and electron intensity

data associated with the crossing of the bow shock and

magnetopause.

Figure 12. Seven days of observations on the inbound leg of the

encounter trajectory through the sunward portion of the

magnetodisc.

Figure 13. Absolute omnidirectional intensities of electrons as

observed in the inner magnetosphere of Jupiter.

Figure 14. Six days of observations on the outbound leg of the

encounter trajectory through the pre-dawn portion of the

magnetodisc.

Figure 15. Six further days of observations on the outbound leg

of the encounter trajectory through the pre-dawn portion

of the magnetodisc.

Figure 16. Examples of the magnetic field nulls that occur near

the mid-point of the magnetodisc at times of maximum

particle intensity.

Figure 17. Time profile of intensity of protons $0.6 < E_p < 3.4$

MeV as observed with a thin, single element solid state

detector on Pioneer 11. This interplanetary event is

identified with the drop-out of intensity in the magneto-

disc 0500-1100/December 1 as observed with Pioneer 10

(Figure 12).

Figure 18. Four examples of angular distributions of electrons

in the Jovian magnetodisc. The components of the local

magnetic vector are referenced to a right-handed inertial

polar coordinate system whose axis is parallel to the

rotational axis of the planet. The $\theta = 0°$ axis points

northward.

Figure 19. A polar plot of the radial distances and System III

longitudes of the minima in the counting rate of detector C

during the inbound traversal of the magnetodisc and of the

maxima in the counting rate of detector G during the out-

bound traversal of the magnetodisc (cf. Figures 12, 14,

and 15). λ_{III} is measured clockwise from the +X-axis.

The sense of rotation of the planet is counterclockwise.

If the magnetodisc were rigidly attached to the planet

with pole at $\lambda_{III} = 224°$, all points would lie along the

radial line marked 44°.

Figure 20. Inbound and outbound counting rates of detector C

$(E_e > 21$ MeV) as a function of L for the Smith et al. [1974]

model of the Jovian magnetic field. All rates are
corrected to magnetic equatorial values assuming a
pitch angle distribution $j \propto \sin^4 \alpha$.

Figure 21. A plot similar to Figure 20 but for a different
model of the magnetic field as shown.

Figure 22. An improved version of Figure 21, assuming a simple
L-dependence of m in the angular distribution
$j \propto \sin^m \alpha$.

Figure 23. A plot similar to Figure 22 for detector D
$(E_e > 31 \text{ MeV})$.

Figure 24. The L-dependence of the differential spectral index
γ in a power law spectrum as derived from the counting
rate ratio C/D. The abscissa is based on a $9.5°$ tilt of
the dipole toward longitude $\lambda_{III} = 230°$.

Figure 25. The L-dependence of the two differential spectral
indices γ_1 (lower pair of curves) for $0.06 < E < 5$ MeV
and γ_2 (upper pair of curves) for $E_e > 5$ MeV. The
abscissa is based on a $9.5°$ tilt of the dipole toward
longitude $\lambda_{III} = 230°$.

A-G70-316-I

Figure 1

A-G69-677

END VIEW

Figure 2

A-G70-592-1

PB SHIELDING

FOAM

Mg COVER

Mg HOUSING

G

1"

Z

X

Figure 3

UNIVERSITY
OF
IOWA

PIONEER F/G
PACKAGE

D,E,F

A

B

G

Z

Y

X
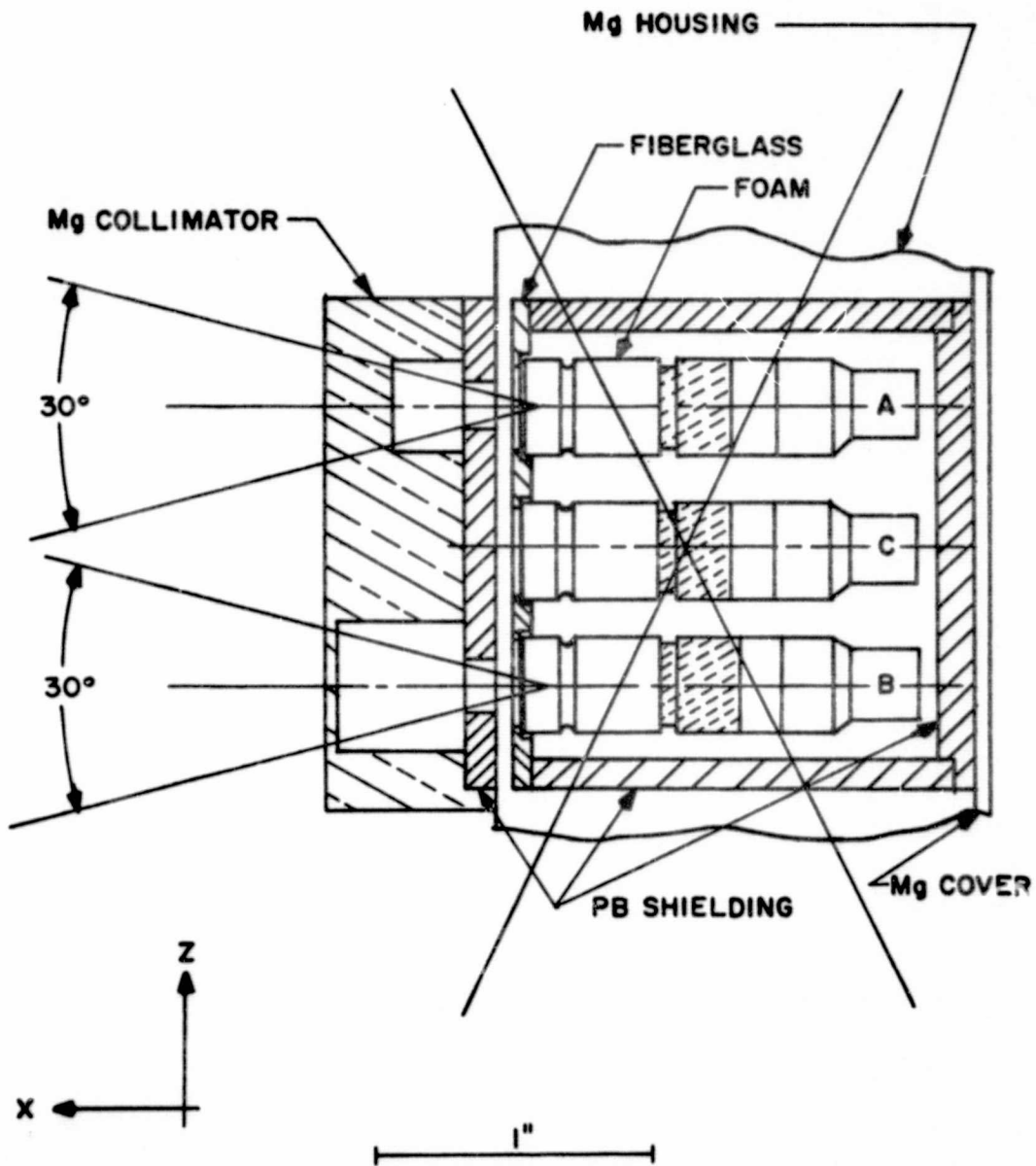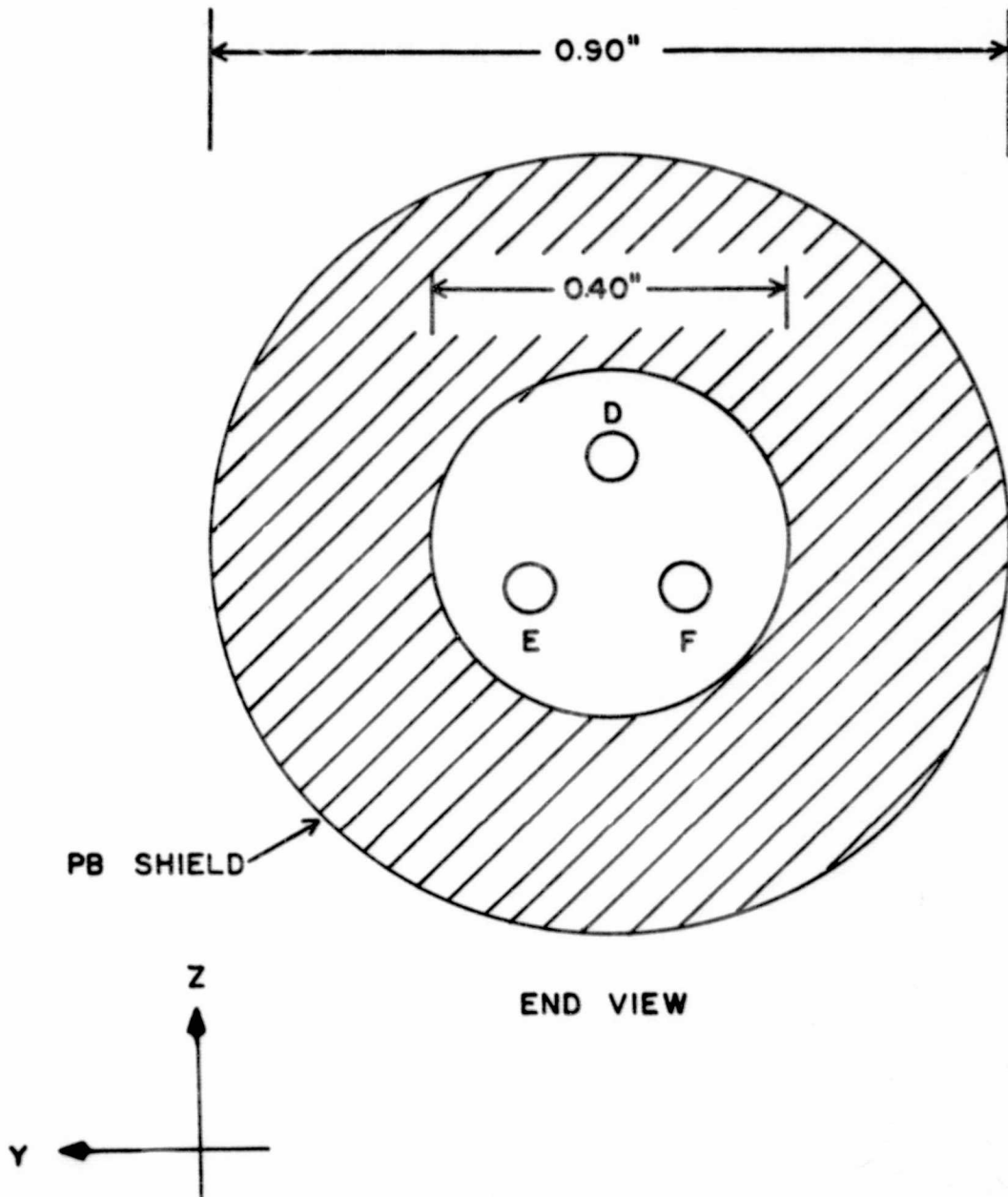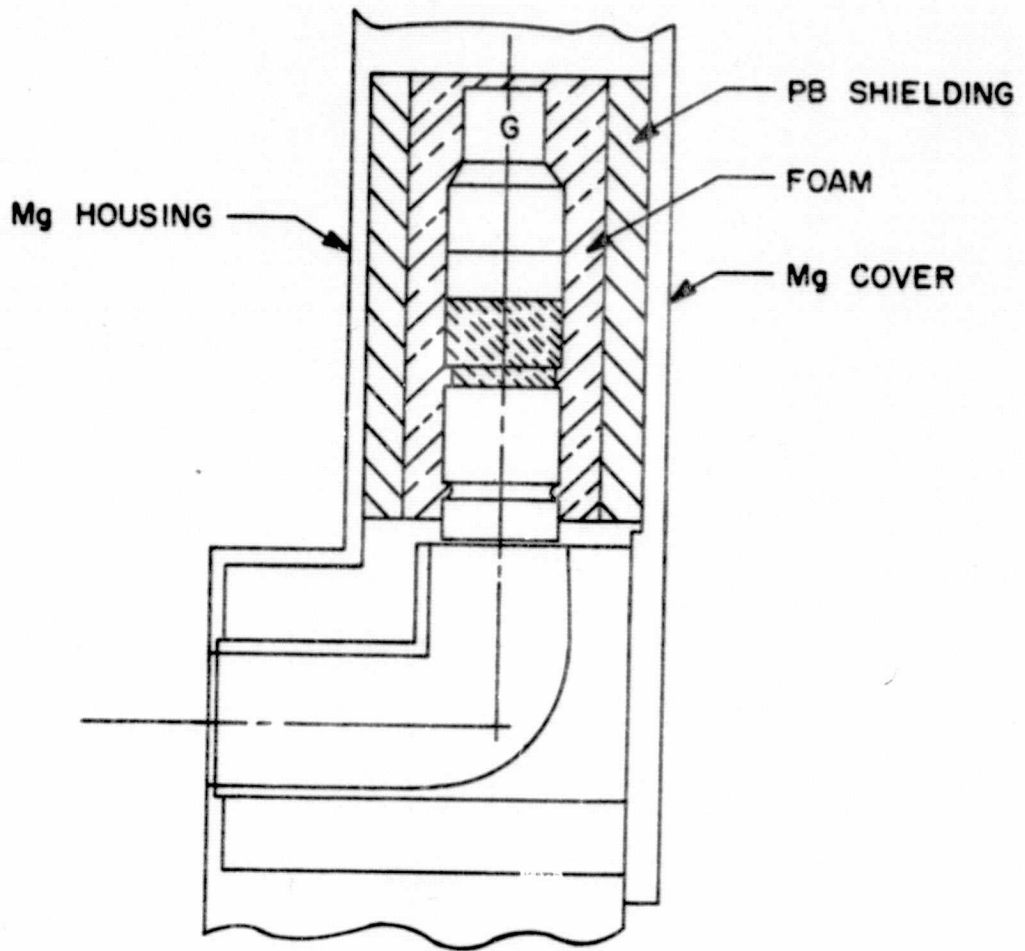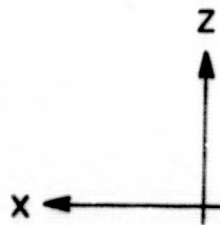
Figure 4
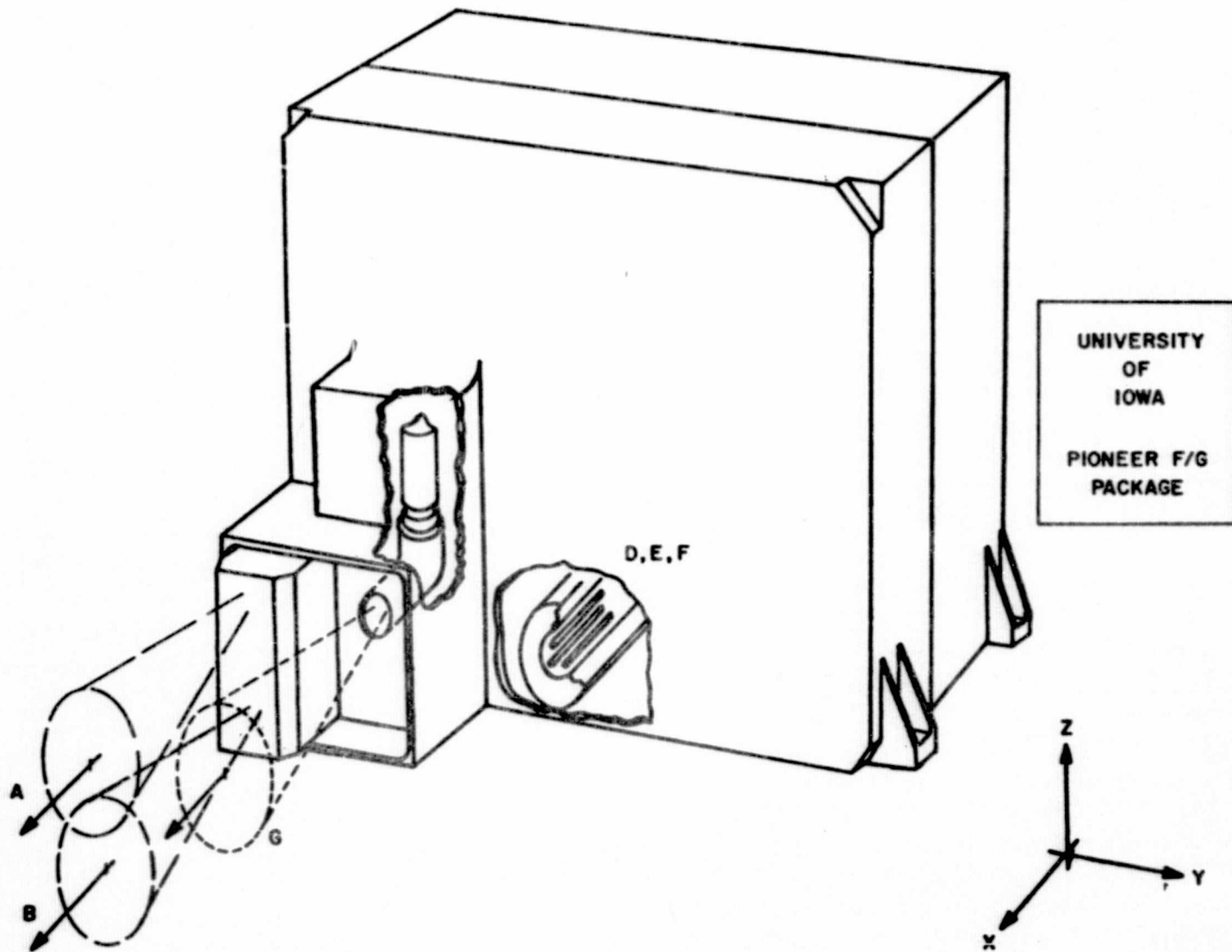
Figure 5.

PIONEER 10
PROTON RESPONSES
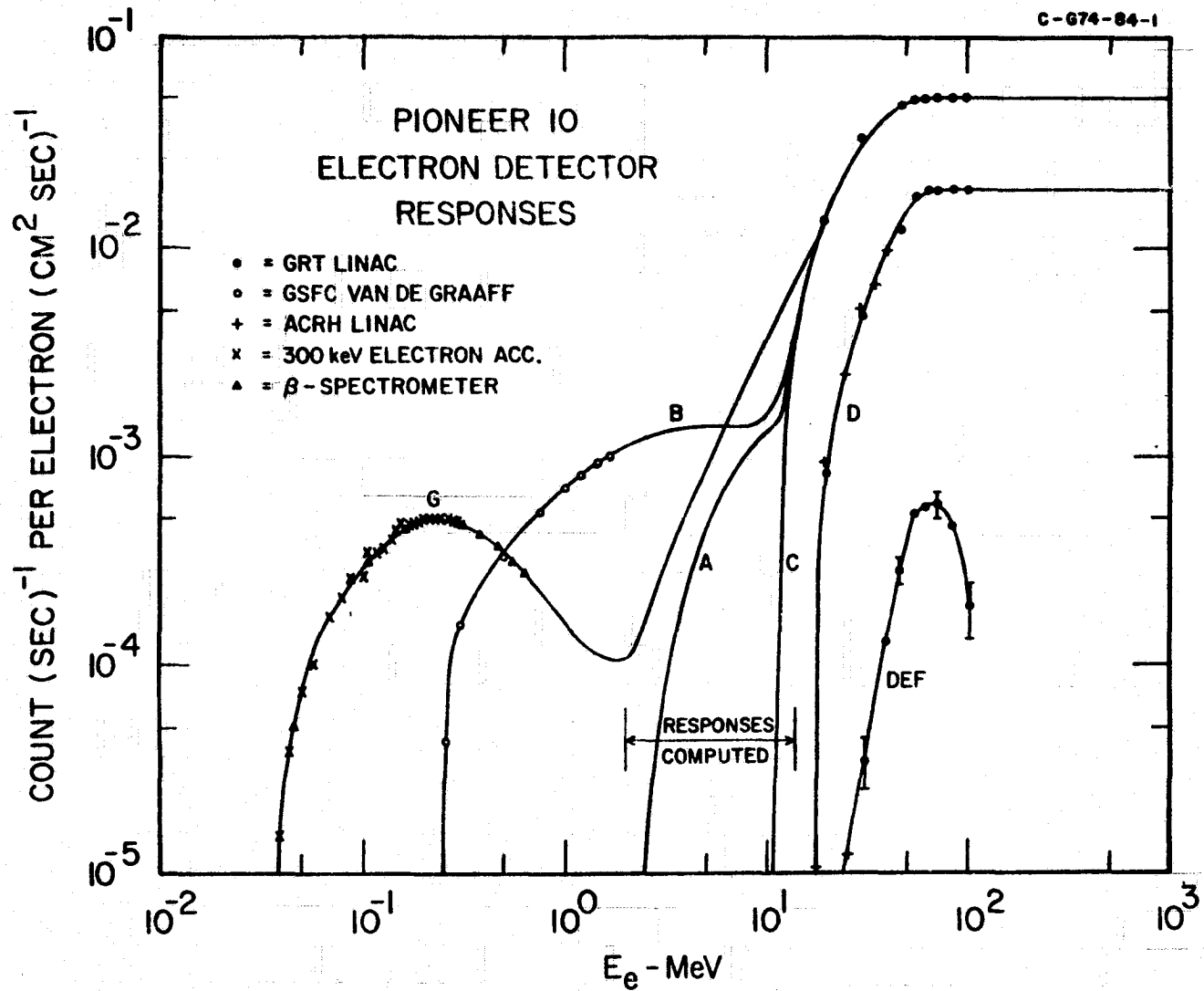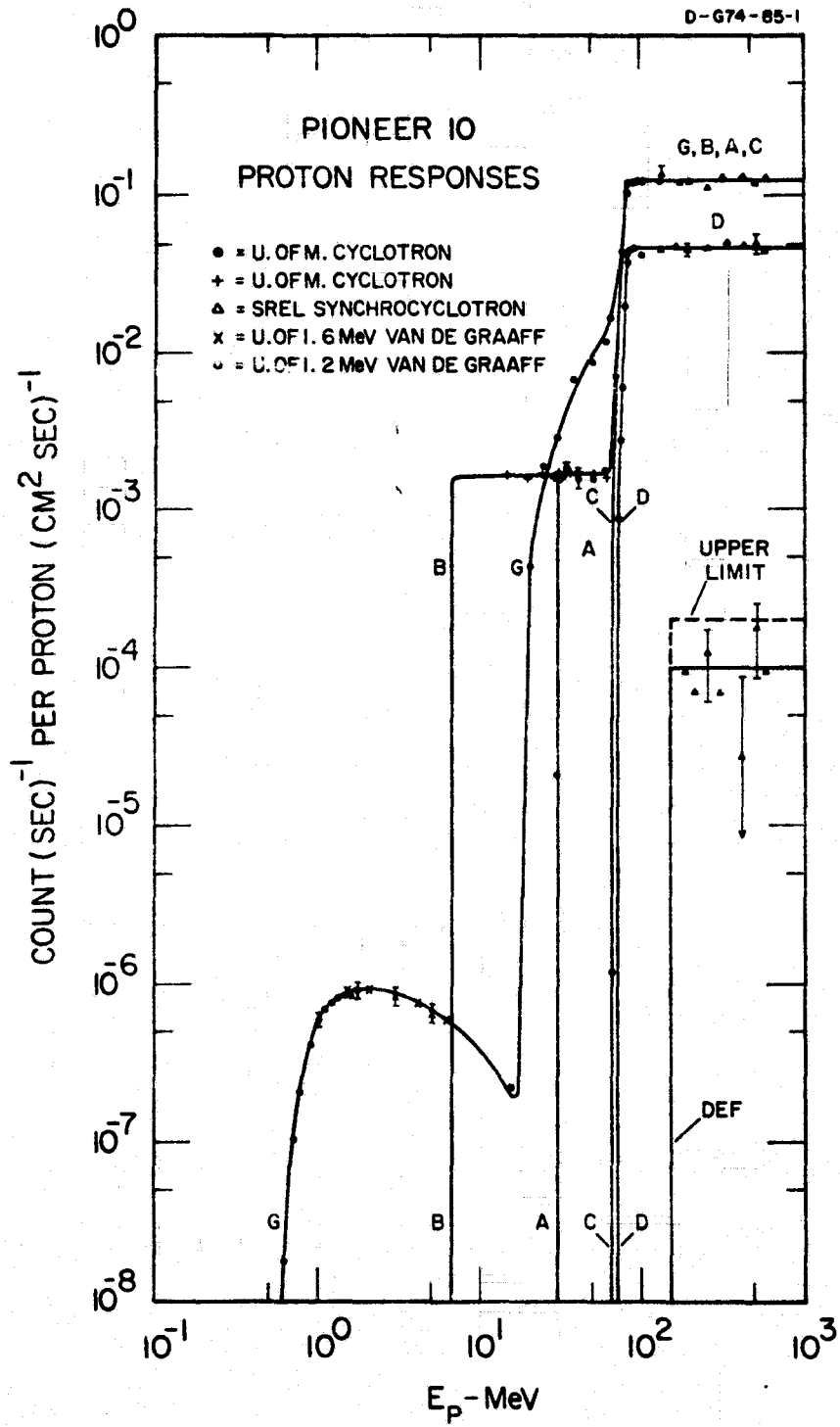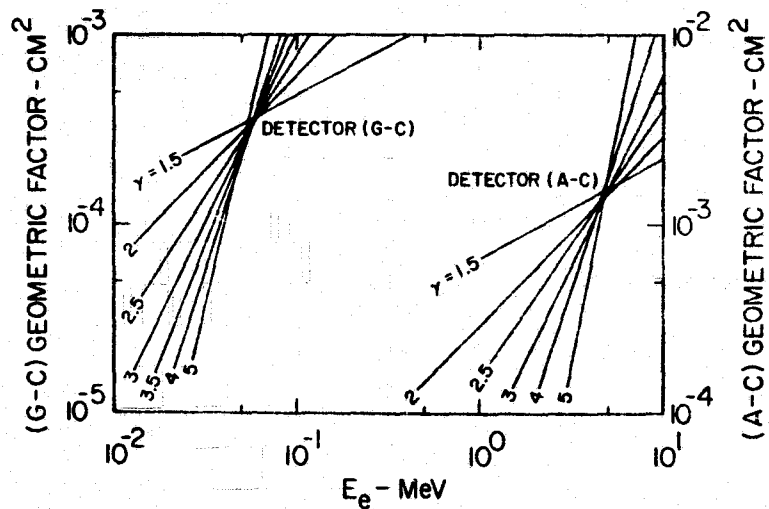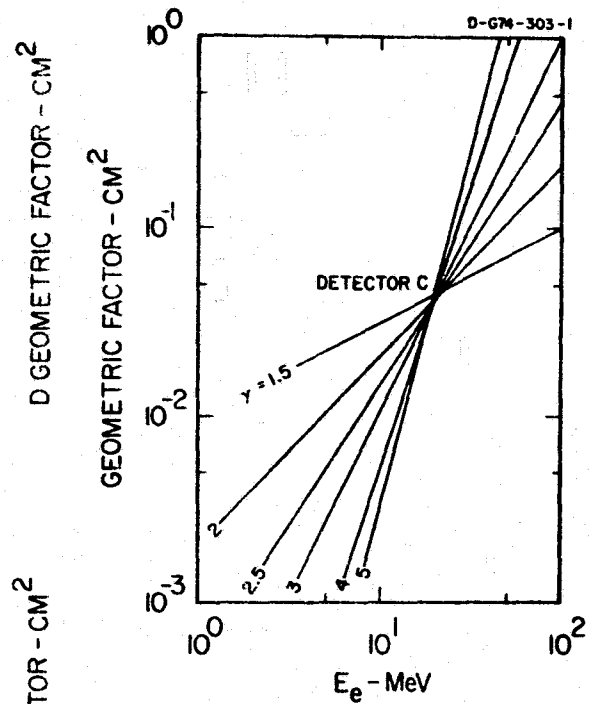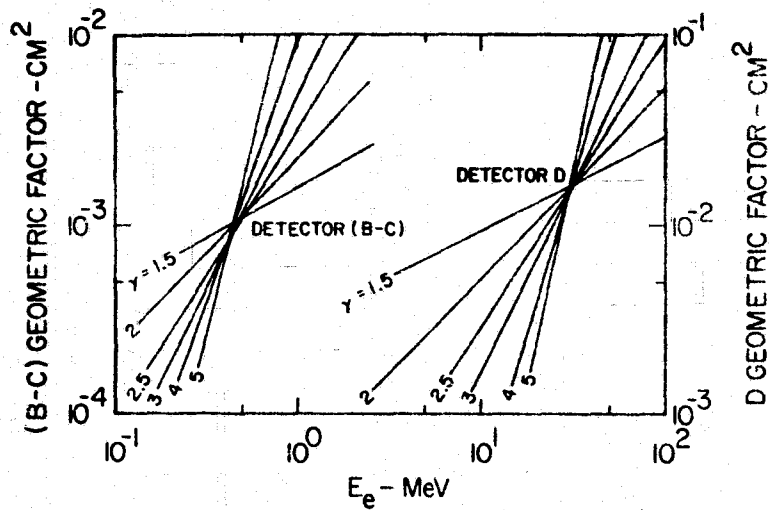
Figure 6

UNIVERSITY OF IOWA
PIONEER 10 DETECTOR
GEOMETRIC FACTORS

$$G(E,\gamma) = \frac{\int_0^\infty dE \cdot R(E) \cdot E^{-\gamma}}{\int_E^\infty E^{-\gamma} dE}$$

R = DETECTOR RESPONSE FUNCTION

Figure 7

Figure 8

Figure 9

D-G74-326
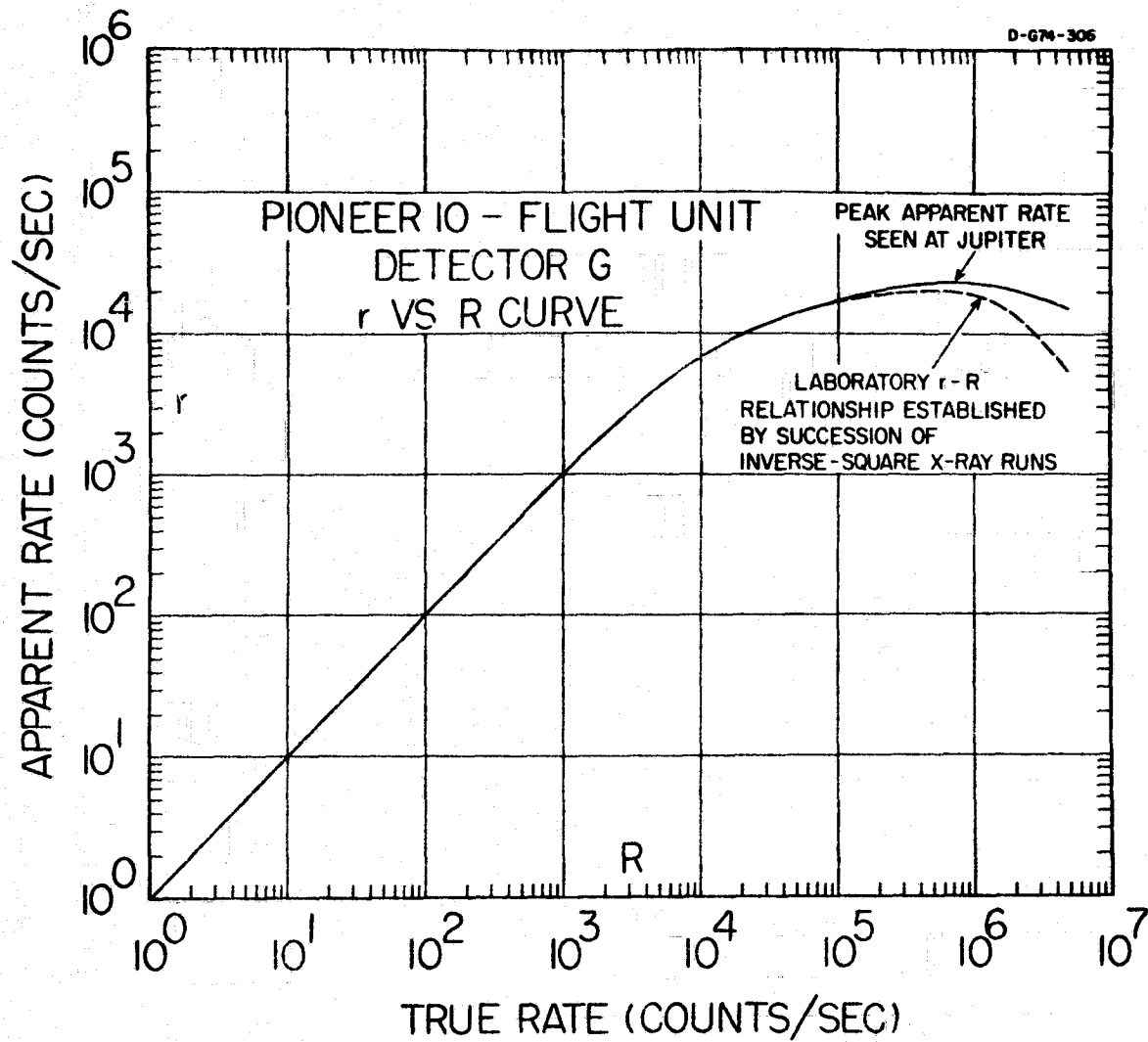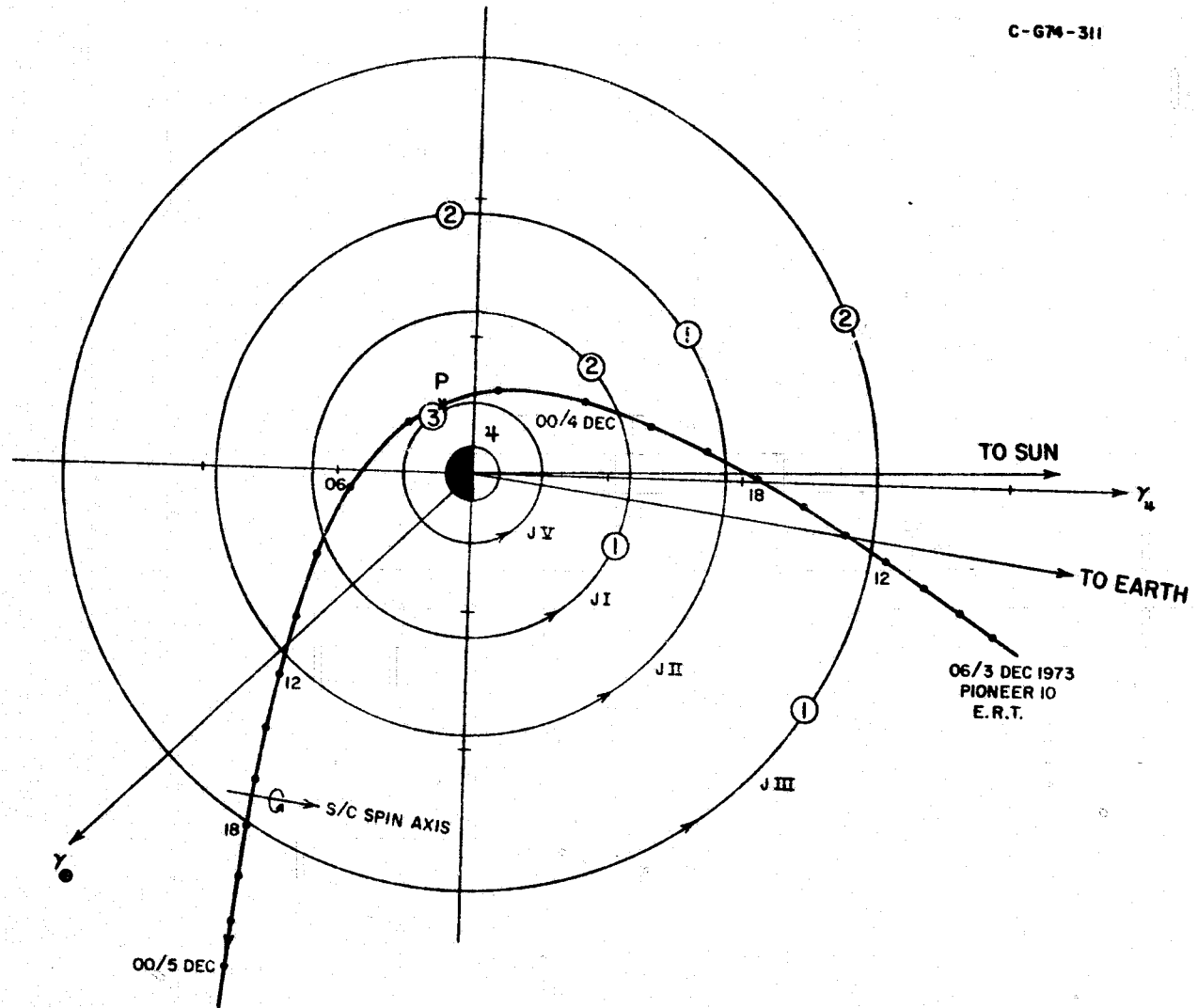
PIONEER IO ENCOUNTER
MAGNETIC MERIDIAN PLANE PROJECTION

CENTERED DIPOLE $\begin{cases} \text{TILT} = 9.5° \\ \lambda_{\text{III}} \ (1957) = 230° \end{cases}$
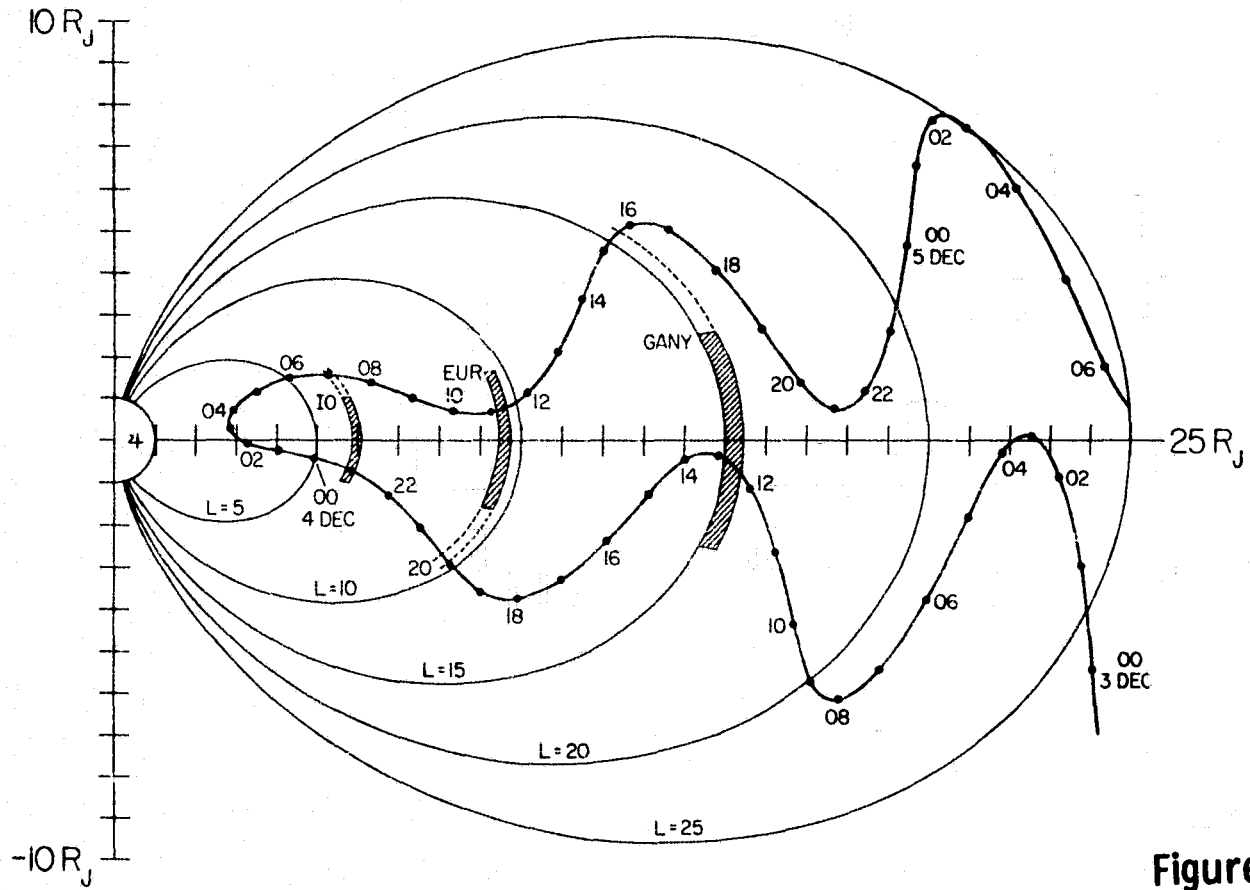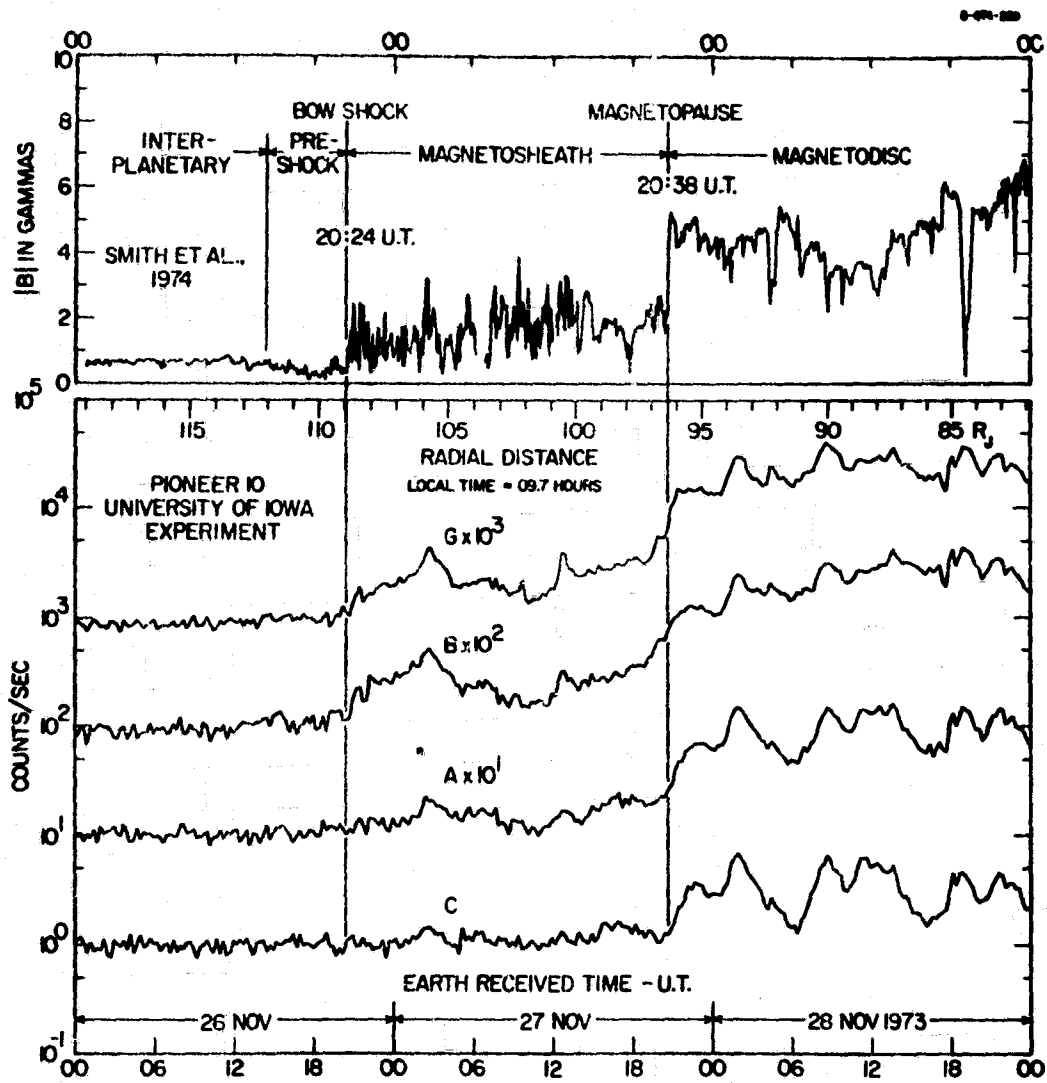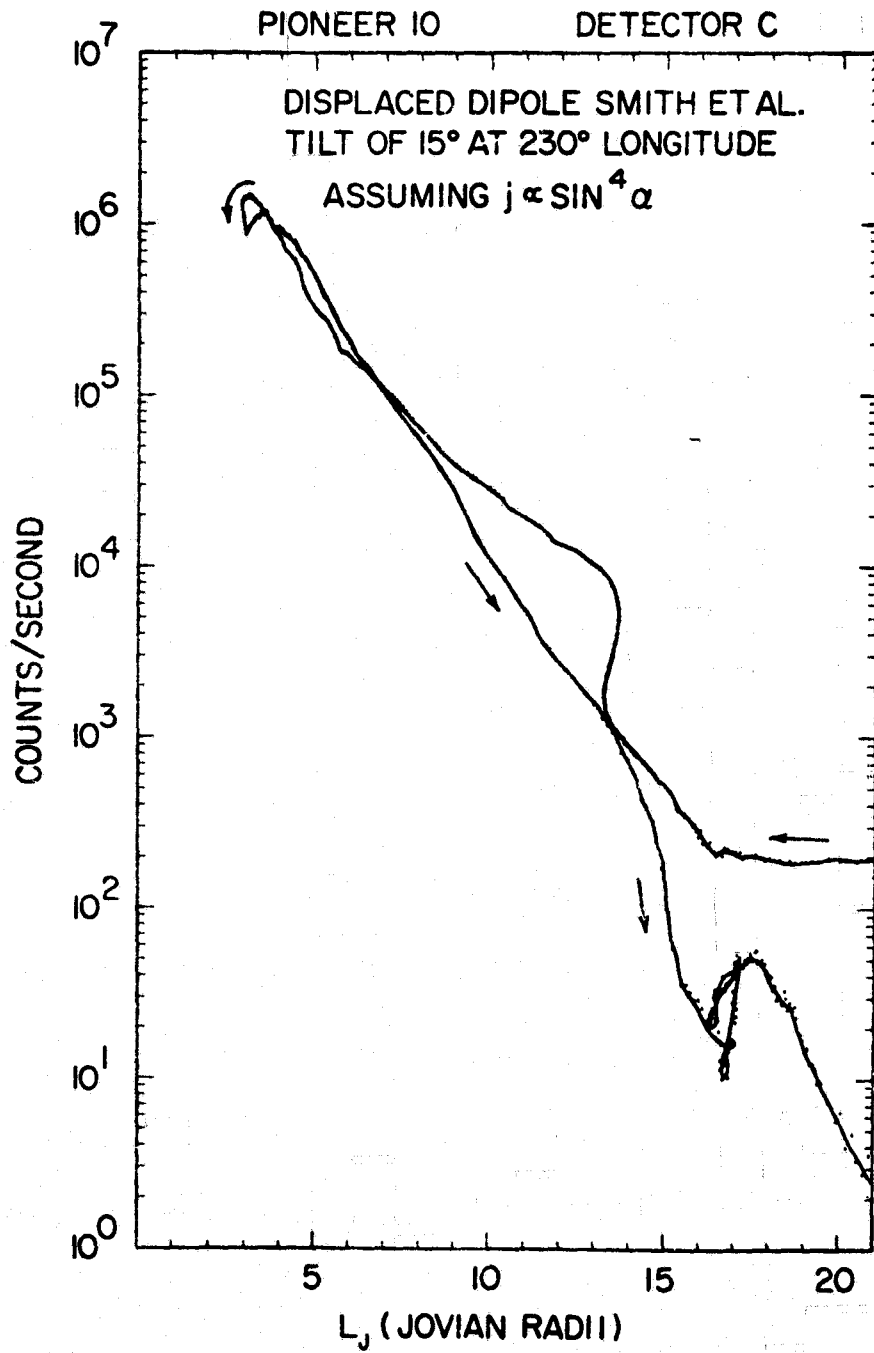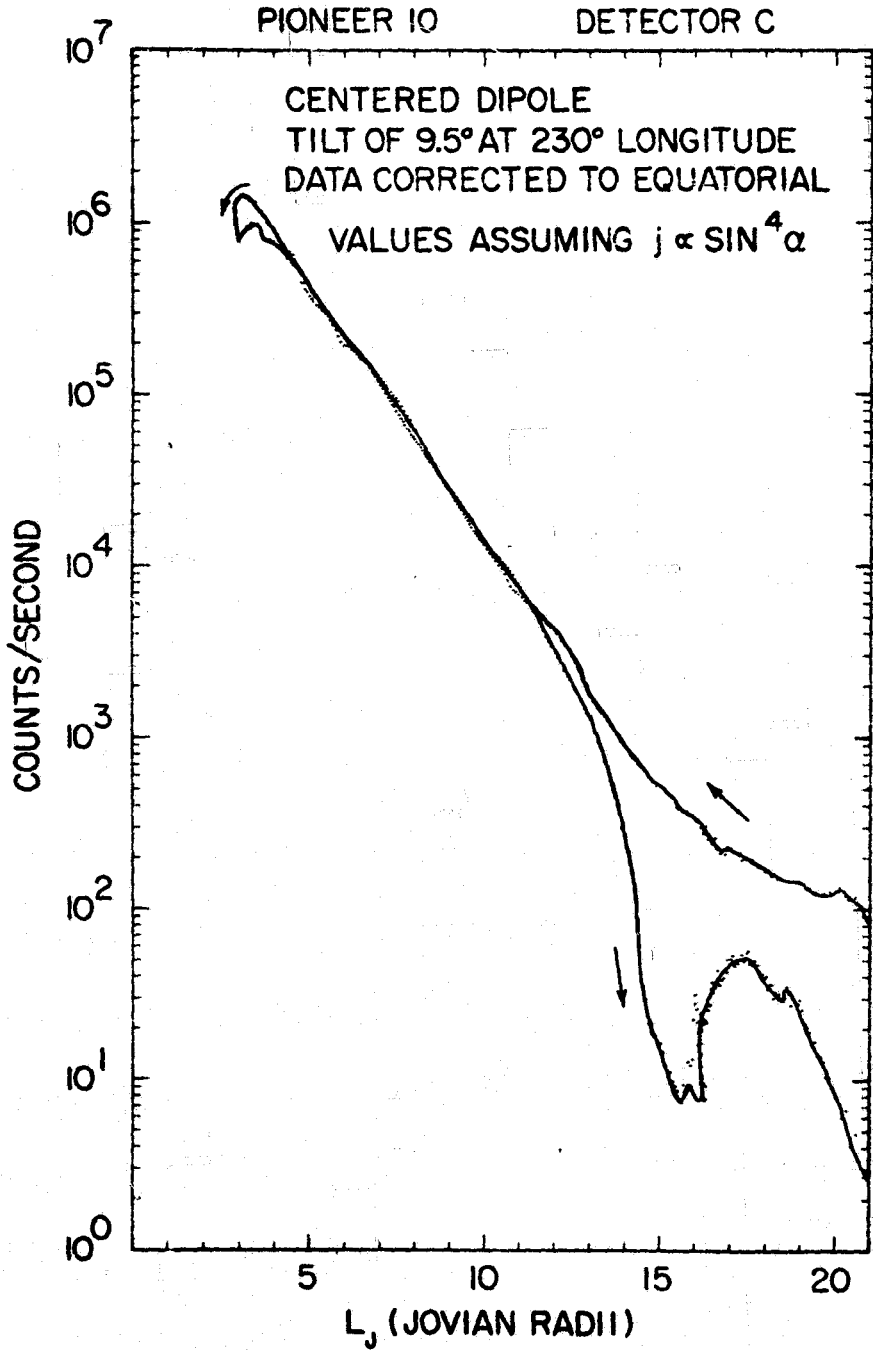
Figure 10

Figure 11
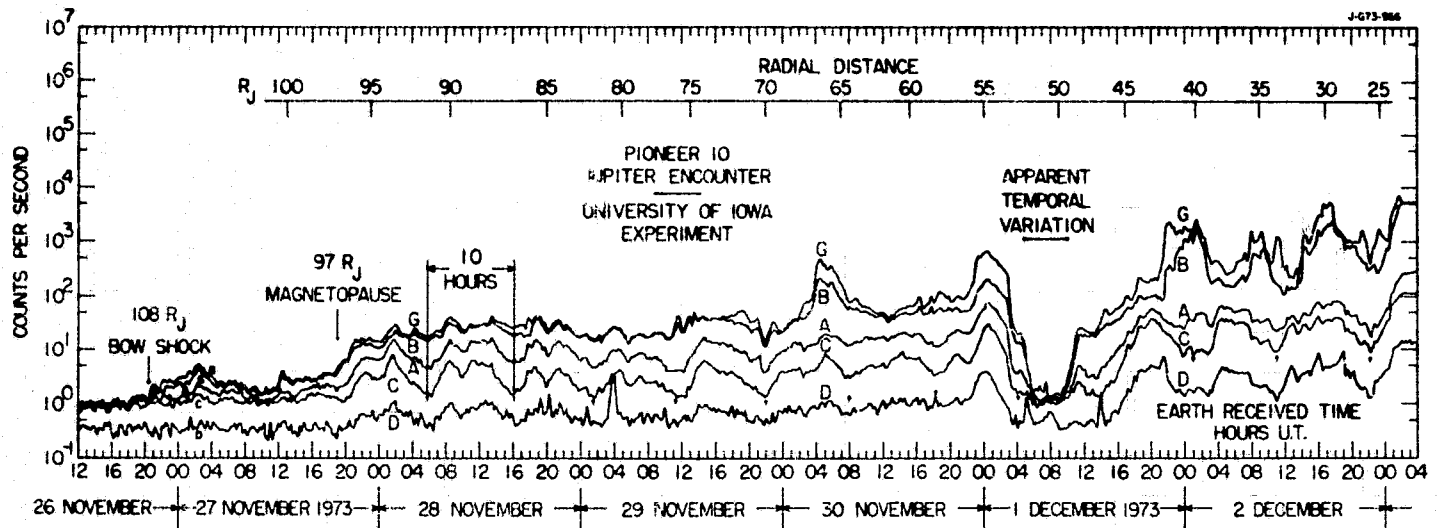
Figure 12
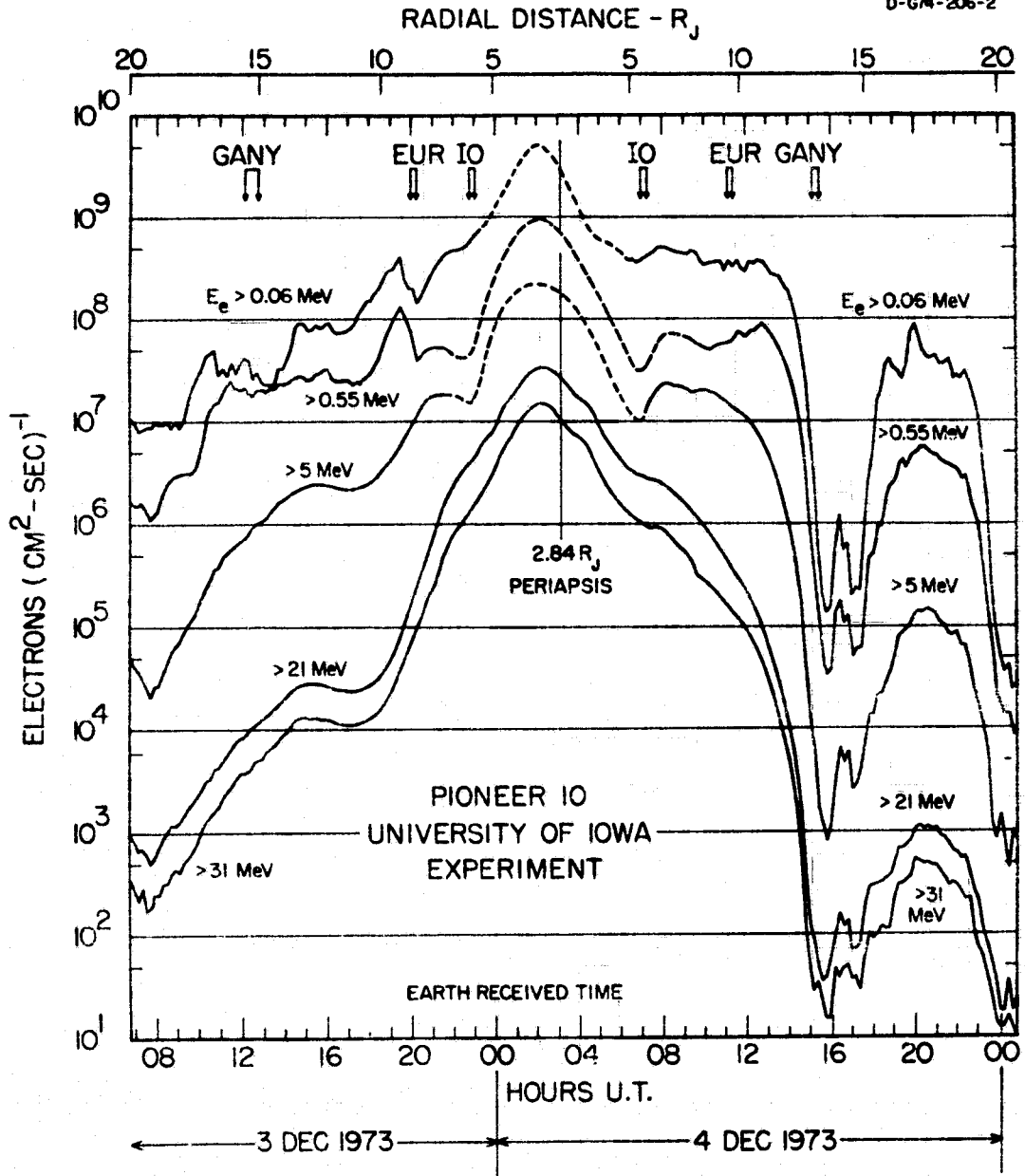
Figure 13

RADIAL DISTANCE

PIONEER 10
JUPITER ENCOUNTER

UNIVERSITY OF IOWA
EXPERIMENT

COUNTS PER SECOND

EARTH RECEIVED TIME   HOURS U.T.

5 DECEMBER 1973 — 6 DECEMBER — 7 DECEMBER — 8 DECEMBER — 9 DECEMBER — 10 DECEMBER 1973

71>

Figure 14

Figure 15

72<

Figure 16

73<

PIONEER II
UNIVERSITY OF IOWA EXPERIMENT

PROTONS: $0.6 < E_p < 3.4$ MeV

$g = 4.1 \times 10^{-2}$ CM^2 SR

02:30/3 DEC

09:55/4 DEC

21^h

BKG.

46^h

DAY OF YEAR 1973

COUNTS/SEC

1.0

0.1

0.01

336   337   338   339   340

74>

Figure 17

PIONEER 10

Figure 18

INBOUND
MINIMA-C

λ_{III}

44°

ω

(r, λ_{III}) POLAR PLOT

I DIV. = 20 R_J

OUTBOUND
MAXIMA-G

JOVIAN MAGNETODISC

Figure 19

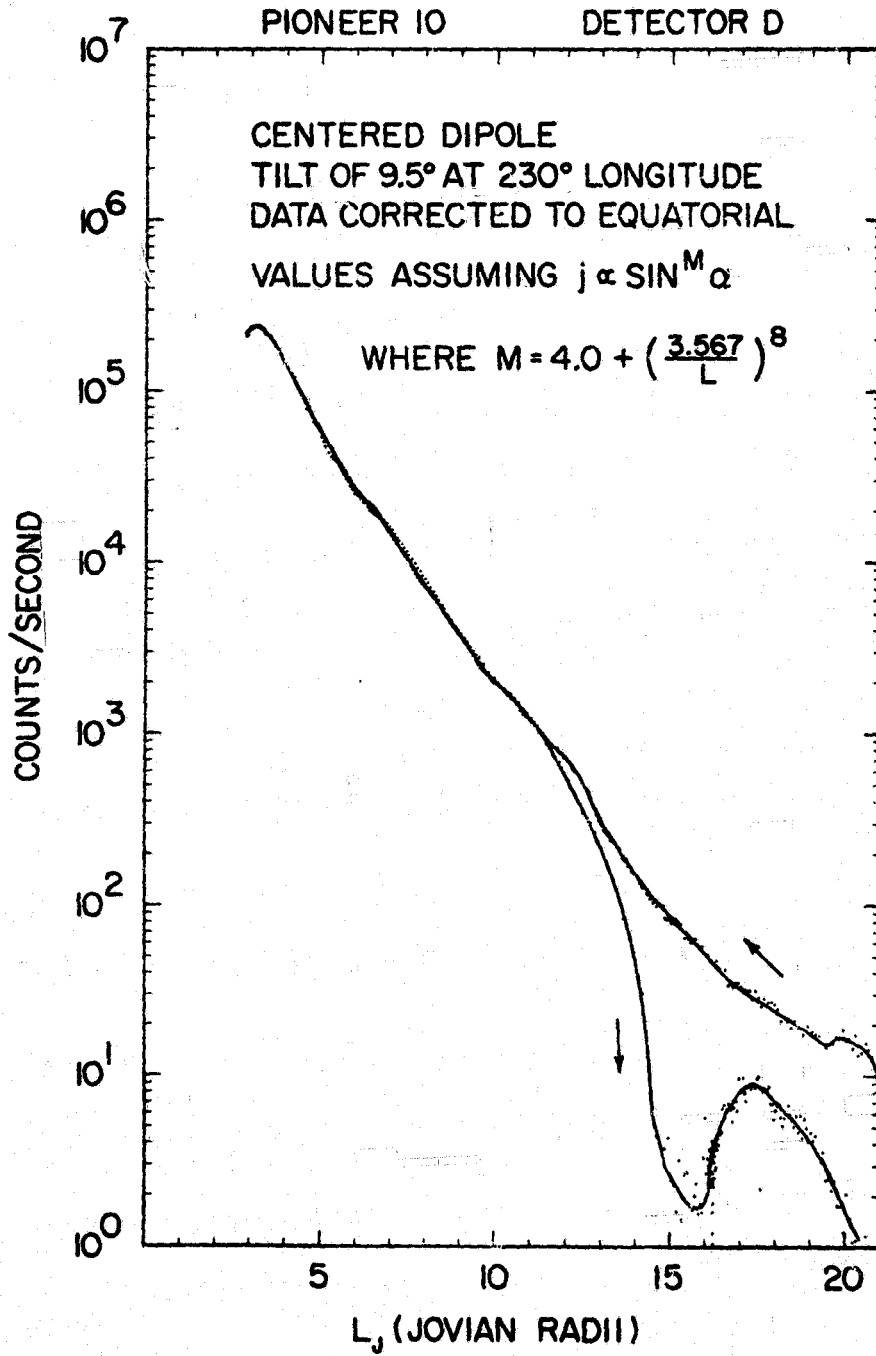Figure 20

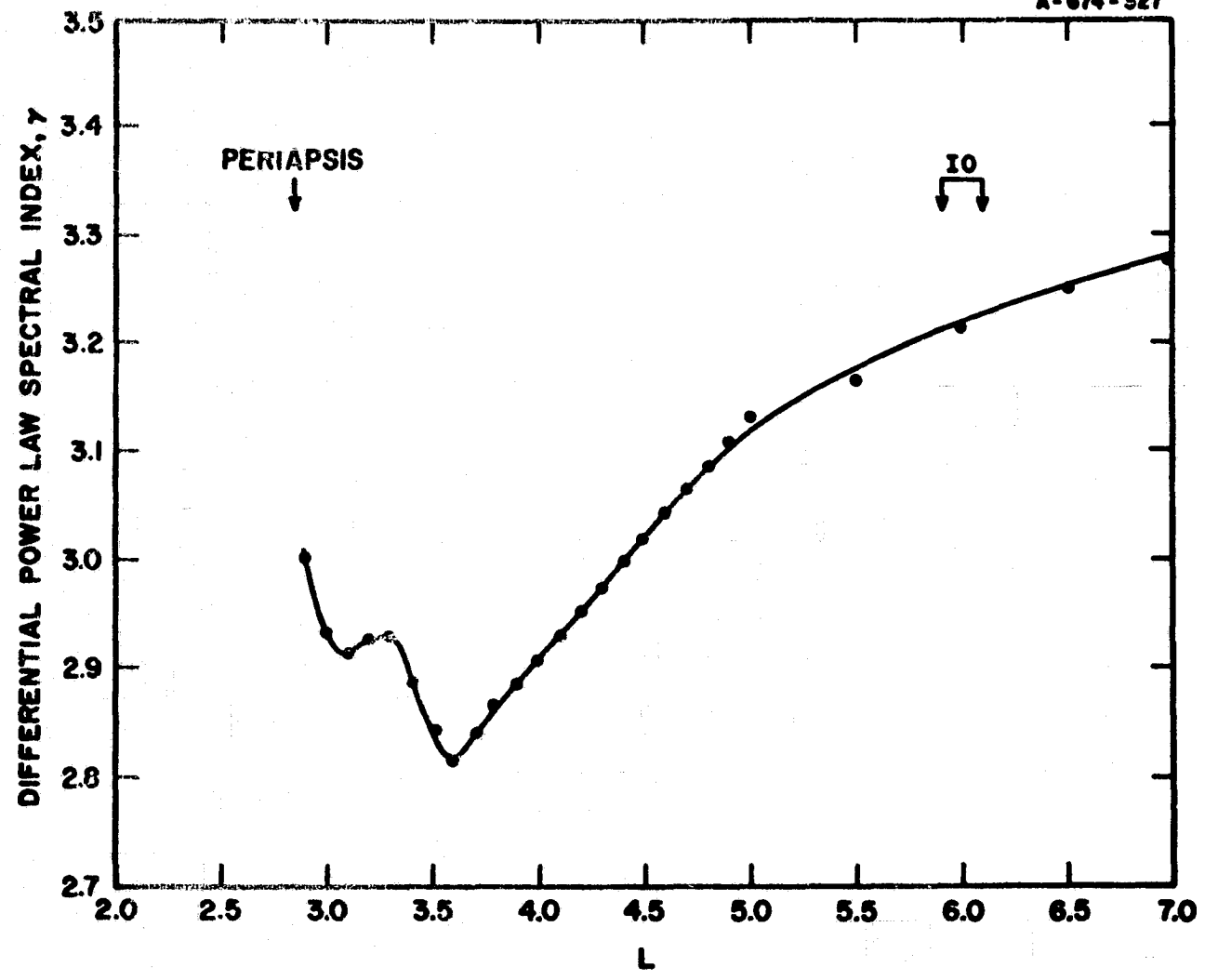Figure 21
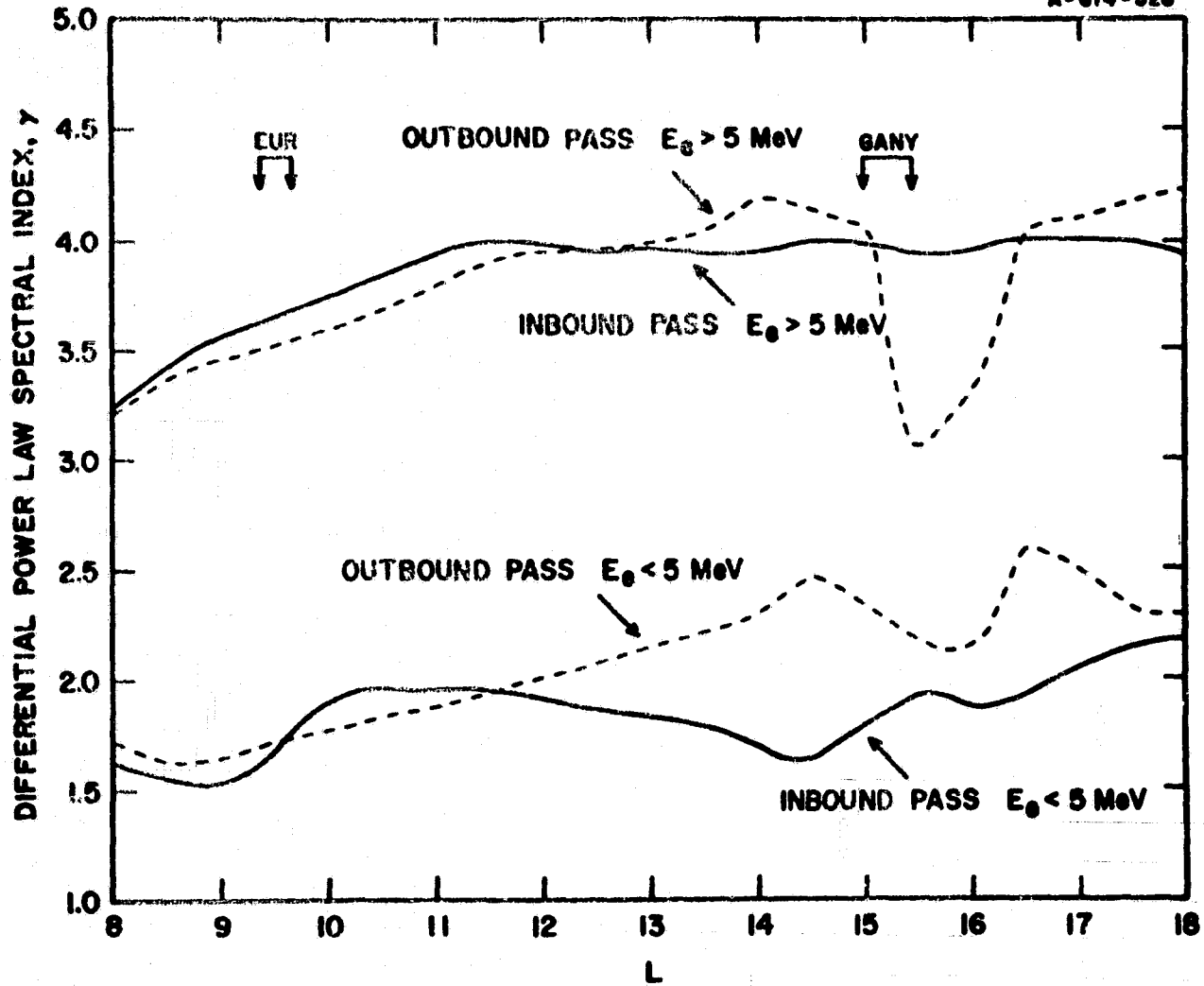
C-G74-318
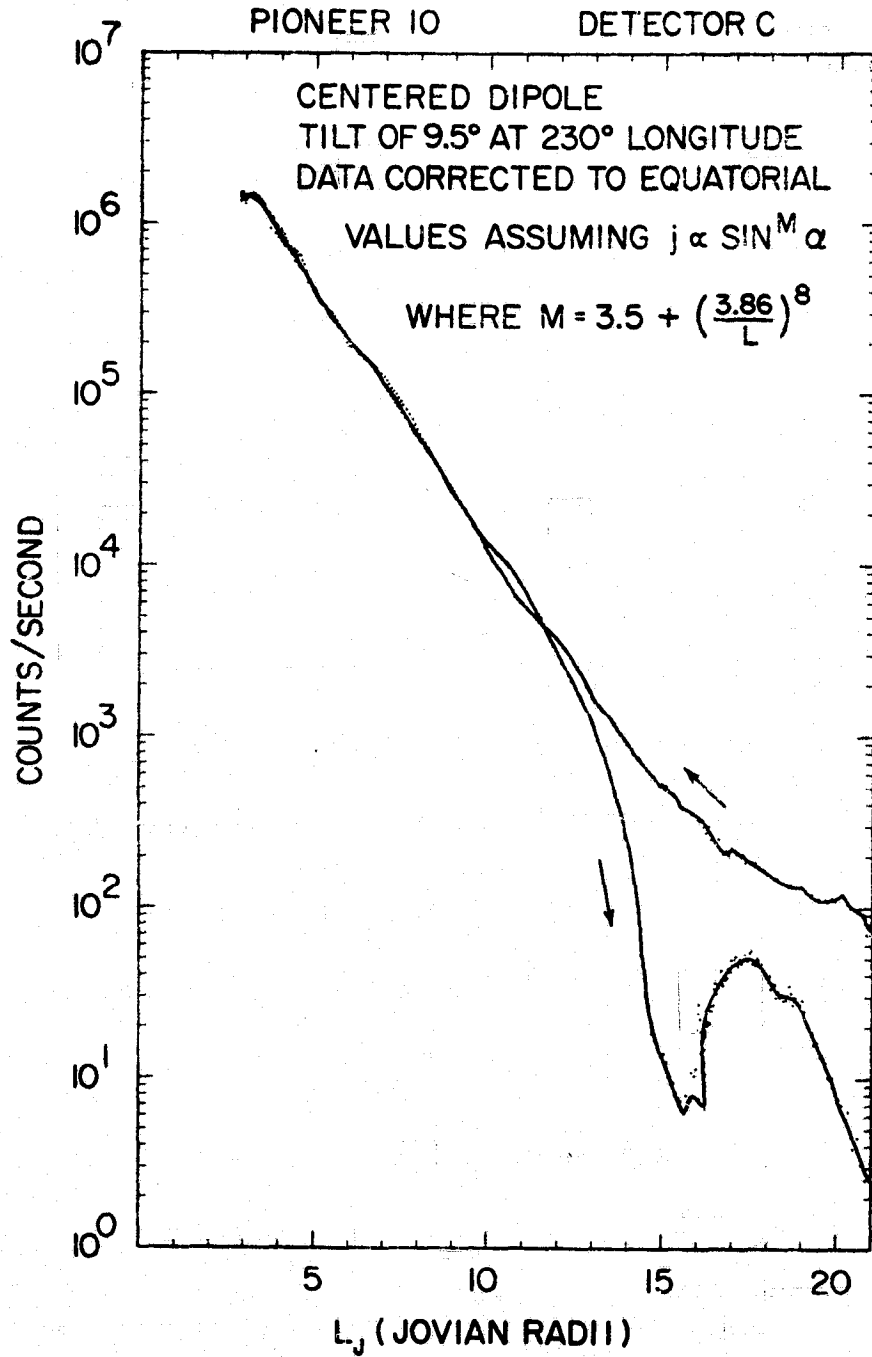
Figure 22

Figure 23

Figure 24

Figure 25

83<

The Magnetosphere of Jupiter as Observed with Pioneer 10.
Part II: Non-Rigid Rotation of the Magnetodisc

by

C. K. Goertz,[*] T. G. Northrop,[**]
and M. F. Thomsen

Department of Physics and Astronomy
The University of Iowa
Iowa City, Iowa 52242

May 1974

ABSTRACT

The maximum count rates of energetic particles are observed
earlier on the inbound pass and later on the outbound pass than
one would expect if the Jovian magnetodisc rotated rigidly with
the planet. This lead and lag cannot be explained by the observed
azimuthal distortion of the Jovian magnetic field alone. The
foot of a magnetic field in the ionosphere must slip with respect
to Jupiter's surface. The rate of slippage and the electric field
necessary for this is estimated. The electric field may be as
large as 2 volts/meter in the Jovian polar ionosphere.

INTRODUCTION

The 10-hour particle-flux modulation exhibited by the energetic particle measurements aboard Pioneer 10 [Van Allen et al., 1974a; Simpson et al., 1974; Trainor et al., 1974; and Filius and McIlwain, 1974] have been interpreted by those authors as being due to a confinement of the energetic particles near the magnetic equatorial plane, which oscillates above and below the rotational equatorial plane. This oscillation is caused by the tilt between Jupiter's magnetic dipole axis and spin axis.

The maximum count rates should then occur when the magnetic latitude of Pioneer 10 is a minimum, i.e., when it is at a Jovian longitude λ III $\approx$ 230° on the inbound pass and at λ III $\approx$ 50° on the outbound pass, based on the model of the Jovian magnetic field described by Smith et al. [1974]. Van Allen et al. [1974b], however, report that the maximum count rates are observed when the spacecraft is at a longitude λ III < 230° on the inbound pass and at λ III > 50° on the outbound pass, i.e., earlier than one would expect on the inbound pass and later on the outbound pass. Figure 1 shows a polar plot of the position of count-rate maxima for the inbound and outbound pass as well as the positions of count rate minima.

The deviations α apparently indicate an azimuthal distortion of the magnetic field from a meridional plane, as indicated in Figure 2. And, indeed, Smith et al. [1974] have reported a systematic sweep back of the magnetic field from meridional planes, as illustrated in Figure 2.

In the following we will show that this is incompatible with Van Allen's observations if we assume that the foot of a field line is tied to the planet, and therefore conclude that it slips.

MAGNETIC FIELD DISTORTION

In the following we will carry out our calculations in a coordinate system having the z-axis along the magnetic dipole; $\hat{\rho}$ is a radial unit-vector in the dipole's equatorial plane and $\hat{\varphi}$ completes a cylindrical coordinate system. A displacement of the outer parts of a field line merely parallel to the magnetic equatorial plane of the dipole cannot account for Van Allen's observations. The displacement must have a component in the rotational equatorial plane. Figure 2 indicates that this requires a displacement not only in the $\hat{\varphi}$ direction of the magnetic coordinate system but also in the $\hat{\rho}$ direction.

The motion of a field line can be thought of as a super-position of a rotation about Jupiter's rotation axis and an up and down motion due to the motion of the dipole with respect to the rotational axis. The outer ends of a field will not immediately adjust to the motion of the dipole but will follow with a time delay Δt

$$\Delta t = \int_{Jupiter}^{Pioneer} \frac{ds}{g} \tag{1}$$

where g is the group velocity of an Alfvén wave and the integral

is taken along the field line passing through Pioneer 10. The group velocity of an Alfvén wave in the non-rotating system is:

$$\vec{g} = \vec{w} + v_A \vec{B}/B \tag{2}$$

where $\vec{w}$ is the magnetohydrodynamic drift velocity of a blob of plasma tied to the magnetic field. In a time Δt the foot of the field line moves by $(\Delta\varphi)_0 = (g_\varphi)_0 \Delta t/\rho_0$, provided B_φ vanishes at the foot of the field line. The outer end lags behind by $\Delta\lambda$ where

$$\Delta\lambda = \frac{(g_\varphi)_0}{\rho_0} \Delta t - \varphi \tag{3}$$

where φ is the angular motion of the outer end in the time Δt and

$$\frac{d\Delta\lambda}{d\rho} = \frac{(g_\varphi)_0}{\rho_0} \frac{d\Delta t}{d\rho} - \frac{d\varphi}{d\rho} = \frac{(g_\varphi)_0}{\rho_0} \frac{d\Delta t}{d\rho} - \frac{1}{\rho} \frac{g_\varphi}{g_\rho} \tag{4}$$

For a conducting plasma we have (in the non-rotating frame):

$$\nabla \times (\vec{w} \times \vec{B}) = \partial\vec{B}/\partial t . \tag{5}$$

In the magnetic frame the φ derivatives of the components of $\vec{B}$ vanish and a solution of Equation (5) is

$$w_\rho = k\, B_\rho \quad , \quad w_z = k\, B_z \quad , \quad w_\varphi - k\, B_\varphi = a\, \rho \quad ,$$

$$\frac{\partial \vec{B}}{\partial t} = - \vec{B}\, \frac{\partial a}{\partial \varphi} \tag{6}$$

if the change of magnetic field $\partial\vec{B}/\partial t$ can be attributed to rotation of the source of $\vec{B}$ with the planet. k is a function of position and a is constant along a field line. k represents mass flow away from the planet. At the foot $(B_\varphi)_0 = 0$ and thus:

$$a(\varphi)\, \rho_0 = (w_\varphi)_0 \quad .$$

Since

$$\Delta t = \int_{\rho_0}^{\rho} \frac{d\rho'}{g_\rho}$$

and

$$g_\varphi = w_\varphi + v_A\, \frac{B_\varphi}{B} = \frac{\rho}{\rho_0}\, (w_\varphi)_0 + k B_\varphi = v_A\, \frac{B_\varphi}{B}$$

$$= \frac{\rho}{\rho_0}\, (w_\varphi)_0 + w_\rho\, \frac{B_\varphi}{B_\rho} + v_A\, \frac{B_\varphi}{B} \quad ,$$

$$\frac{d\Delta\lambda}{d\rho} = \frac{(g_\varphi)_0}{\rho_0}\frac{1}{g_\rho} - \frac{(w_\varphi)_0}{\rho_0}\frac{1}{g_\rho} - \frac{1}{\rho}\frac{w_\rho}{g_\rho}\frac{B_\varphi}{B_\rho} - v_A\frac{B_\varphi}{B}\frac{1}{g_\rho}\frac{1}{\rho}$$

$$= -\frac{1}{\rho}\frac{B_\varphi}{B_\rho}[w_\rho + v_A\frac{B_\rho}{B}]\frac{1}{g_\rho} = -\frac{1}{\rho}\frac{B_\varphi}{B_\rho} \quad . \tag{7}$$

This is the equation of a magnetic field line in the magnetic coordinate system. The result (7) is obvious if there is rigid co-rotation and no mass flow, but we have now established its general validity.

We have analyzed the magnetic field data given to us by Smith. Figure 3 shows the radial and azimuthal magnetic field components as well as the ratio $B_\varphi/\rho B_\rho$, all measured in a (tilted) magnetic frame, with a tilt angle of 15°. A positive value for $B_\varphi/\rho B_\rho$ indicates a lead. $B_\varphi/\rho B_\rho$, however, is predominantly negative both on the outbound and inbound pass. The occasional positive value is most likely due to numerical uncertainties in the calculations. This result confirms that the outer parts of a magnetic field line always lag the foot of the field line. The data show that B_φ/B_ρ is not a strongly varying function of z, at least in the outer parts of the magnetosphere. Using the smooth curve for $B_\varphi/\rho B_\rho$ in Figure 3 we can easily calculate $\Delta\lambda(\rho)$. The result is shown by the dashed curve in Figure 1. It is quite obvious that this is not sufficient to explain Van Allen's observations. The treatment so far has only

dealt with a difference in longitude between the foot of a field line and the outer parts. Figure 1, however, shows the relative azimuthal deviation of the outer parts of a field line from the surface of Jupiter. Apparently the foot of a field line moves relative to the surface of Jupiter in such a way that it leads the surface on the inbound pass and lags on the outbound pass. In other words, the foot of a magnetic field line is not strictly tied to the planet. It is known that "line-tying" is also only partially effective in the earth's ionosphere (see, e.g., Axford, 1969). The magnetic field data indicate a general lag of the outer parts with respect to the foot of a field line. Thus the observed deviation is

$$\alpha = \Delta\lambda + \beta = - \int_{\rho_0}^{\rho} \frac{1}{\rho'} \frac{B_\varphi}{B_\rho} d\rho' + \beta \quad , \qquad (8)$$

where β is due to a slipping of the foot of a field line with respect to the planet's surface.

INTERPRETATION

The fact that the foot of a field line leads or lags the surface of the planet must be due to the existence of an electric field in the rotation frame of Jupiter because at Jupiter all but the most energetic particles ($E > 10^2$ MeV) move together with the magnetic field at a drift velocity

$$\vec{v}_D = \frac{\vec{E} \times \vec{B}}{B^2} \cdot \cdot \tag{9}$$

If the ionosphere represented a perfect short circuit across the field lines the shorting currents would resist any motion of field lines relative to the planet and the only electric fields which could exist would be due to a $\partial\vec{B}/\partial t$ [Axford, 1969]. Birmingham and Jones [1968] show that the $\partial\vec{B}/\partial t$ due to the rotation of the planet is precisely that required for corotation. Thus the observed deviation from corotation of the feet of field lines with Jupiter must either be due to a steady electric field or a $\partial\vec{B}/\partial t$ not associated with the rotation of Jupiter.

Although we have no a priori reason to believe that the motion is not due to a $\partial\vec{B}/\partial t$, the persistence of the forward motion of the field lines throughout the 6.5 days of the inbound pass seems to

rule out an electric field associated with a $\partial \vec{B}/\partial t$. Since the forward motion is quite large (β changes from 0 to 90° between the early morning and noon) we must require a considerable electric field which, one would imagine, is difficult to achieve with a $\partial \vec{B}/\partial t$ of the order of magnitude produced by Jupiter's rotation. Thus we assume steady state. We can estimate the steady electric field in the following way. From

$$\int_{\rho_0}^{\rho} d\rho' \, \frac{B_\varphi}{\rho' B_\rho}$$

we know that the foot of the field line with Pioneer 10 crossed at a distance r leads the spacecraft by $\Delta\lambda^o(r)$ on the outbound and $\Delta\lambda^i(r)$ on the inbound pass. Assuming that Pioneer 10 crosses essentially the same field lines at a distance r on the inbound and outbound passes (i.e., assuming that the field line is convected around Jupiter with little distention in the radial direction), we find that the foot has moved through an angle of $\beta^o(r) - \beta^i(r)$ whereas the surface has only moved through an angle $\gamma - (\alpha^o - \alpha^i)$ (γ being the angle between the inbound and outbound passes) in the same time (see Figure 4). The surface moves with an angular velocity $\Omega_J = 1.76 \times 10^{-4} \text{ s}^{-1}$ whereas the field line moves with

$$\Omega = \Omega_J \, \frac{\beta^o - \beta^i}{\gamma - (\alpha^o - \alpha^i)} \tag{10}$$

relative to the surface. Then

$$E \approx \Omega \, r \, B(r) \quad .$$

(11)

It is clear that this crude estimate is only justified as long as there is no appreciable stretching of the field lines in the radial direction during their motion from the early morning to noon side of the Jovian magnetosphere, which is probably only true for those field lines which the spacecraft crossed at distances $r < 60 \, R_J$. The electric field in the rotating frame of Jupiter calculated from Equations (10) and (11) is of the order of 10^{-2} V/m. This corresponds to a typical electric field of 2V/m in the Jovian polar ionosphere. The total potential drop across the polar ionosphere and thus across the Jovian magnetosphere may easily be as large as several MeV. Although we do not know what physical mechanism is responsible for electric fields of this magnitude it is tempting to associate it with the magnetic field line merging and reconnection similar to that active in the earth's magnetosphere (see, e.g., Axford, 1969). Then the potential drop across the Jovian magnetosphere is a measure of the maximum energy that can be given to solar wind particles accelerated in the field line reconnection process. This process may explain the relatively large fluxes of energetic particles just inside the magnetosphere which, if they are of solar wind origin, must have gone through an accelerating region.

ACKNOWLEDGMENTS

We thank Dr. J. A. Van Allen for pointing out this problem to us and for many helpful discussions. We also gratefully acknowledge the help of Dr. B. A. Randall in obtaining some of data points displayed in Figure 1. This work was supported in part by the National Aeronautics and Space Administration under contracts Nos. NAS2-5603 and NAS2-6553.

REFERENCES

Axford, W. I., Magnetospheric convection, Rev. of Geophys., 7,
421, 1969.

Birmingham, T. J., and F. C. Jones, Identification of moving magnetic
field lines, J. Geophys. Res., 73, 5505, 1968.

Fillius, R. W., and Carl E. McIlwain, Radiation Belts of Jupiter,
Science, 183, 314, 1974.

Simpson, J. A., D. Hamilton, G. Lentz, R. B. McKibben, A. Magro-
Campero, M. Perkins, K. R. Pyle, A. J. Tuzzolino, and J. J.
O'Gallagher, Protons and electrons in Jupiter's magnetic field:
results from the University of Chicago experiment on Pioneer
10, Science, 183, 306, 1974.

Smith, E. J., L. Davis, Jr., D. E. Jones, D. S. Colburn, P. J.
Coleman, Jr., P. Dyal, and C. P. Sonett, Magnetic field of
Jupiter and its interaction with the solar wind, Science,
183, 305, 1974.

Trainor, J. H., B. J. Teegarden, D. E. Stillwell, F. B. McDonald,
E. C. Roelof, and W. R. Webber, Energetic particle population
in the Jovian magnetosphere: a preliminary note, Science,
183, 311, 1974.

Van Allen, J. A., D. N. Baker, B. A. Randall, M. F. Thomsen, D. D.
Sentman, and H. R. Flindt, Energetic electrons in the
magnetosphere of Jupiter, Science, 183, 309, 1974a.

Van Allen, J. A., D. N. Baker, B. A. Randall, and D. D. Sentman,
The magnetosphere of Jupiter as observed with Pioneer 10:
Part I. Instrument and principal findings, J. Geophys. Res.,
1974b (accompanying paper).

FIGURE CAPTIONS

Figure 1   Polar plot of the positions of count-rate maxima and

minima on the inbound and outbound pass.

Figure 2   The azimuthal distortion of a magnetic field line.

Figure 3   The radial (B_ρ), azimuthal (B_φ) magnetic field com-

ponents, and $B_\varphi/\rho B_\rho$ as a function of radial distance ρ

from the magnetic dipole axis. The dipole axis is

inclined 15° with respect to the rotational axis.

Figure 4   The geometry of the magnetic field distortion and

slippage. The heavy lines indicate the projection of

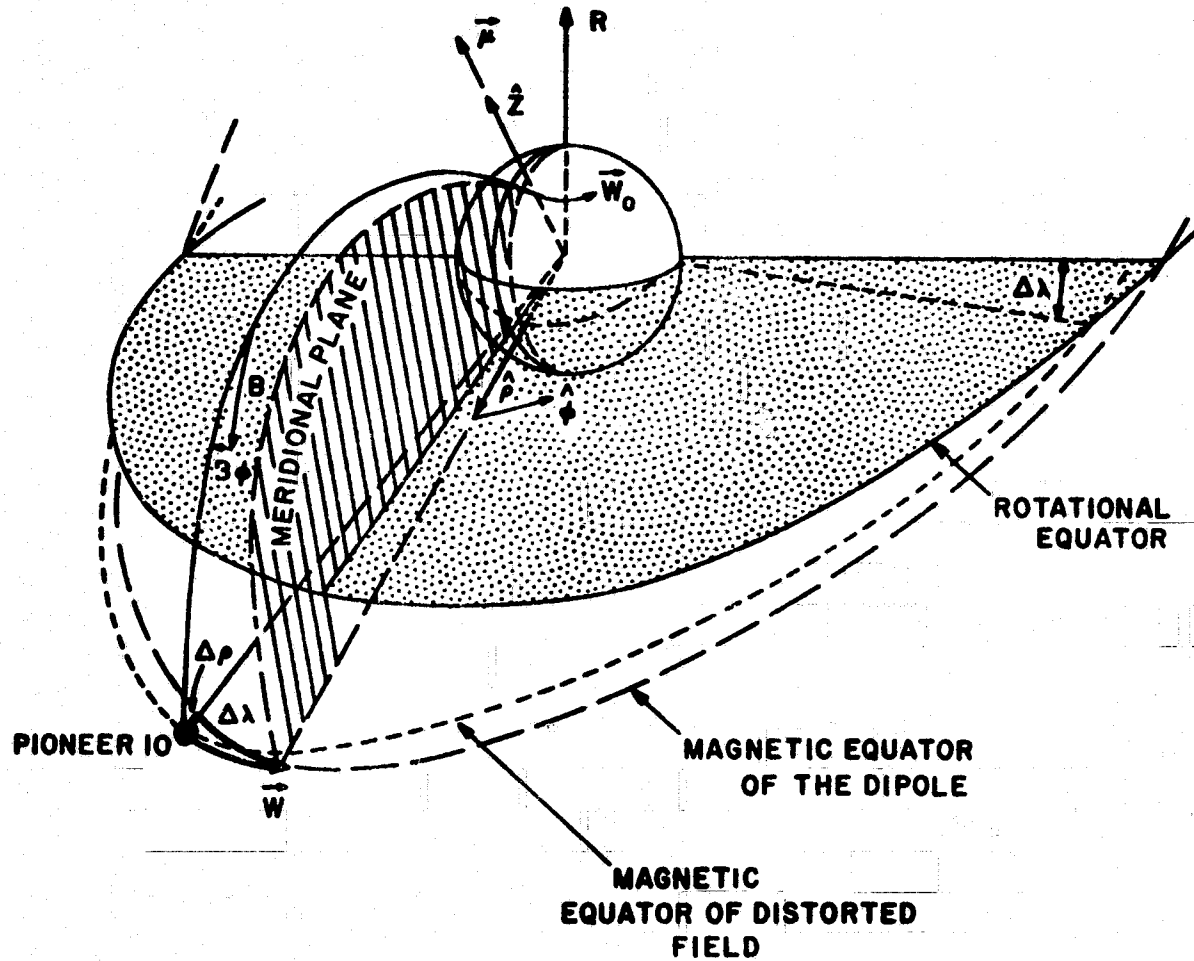the distorted field lines on the ecliptic plane.

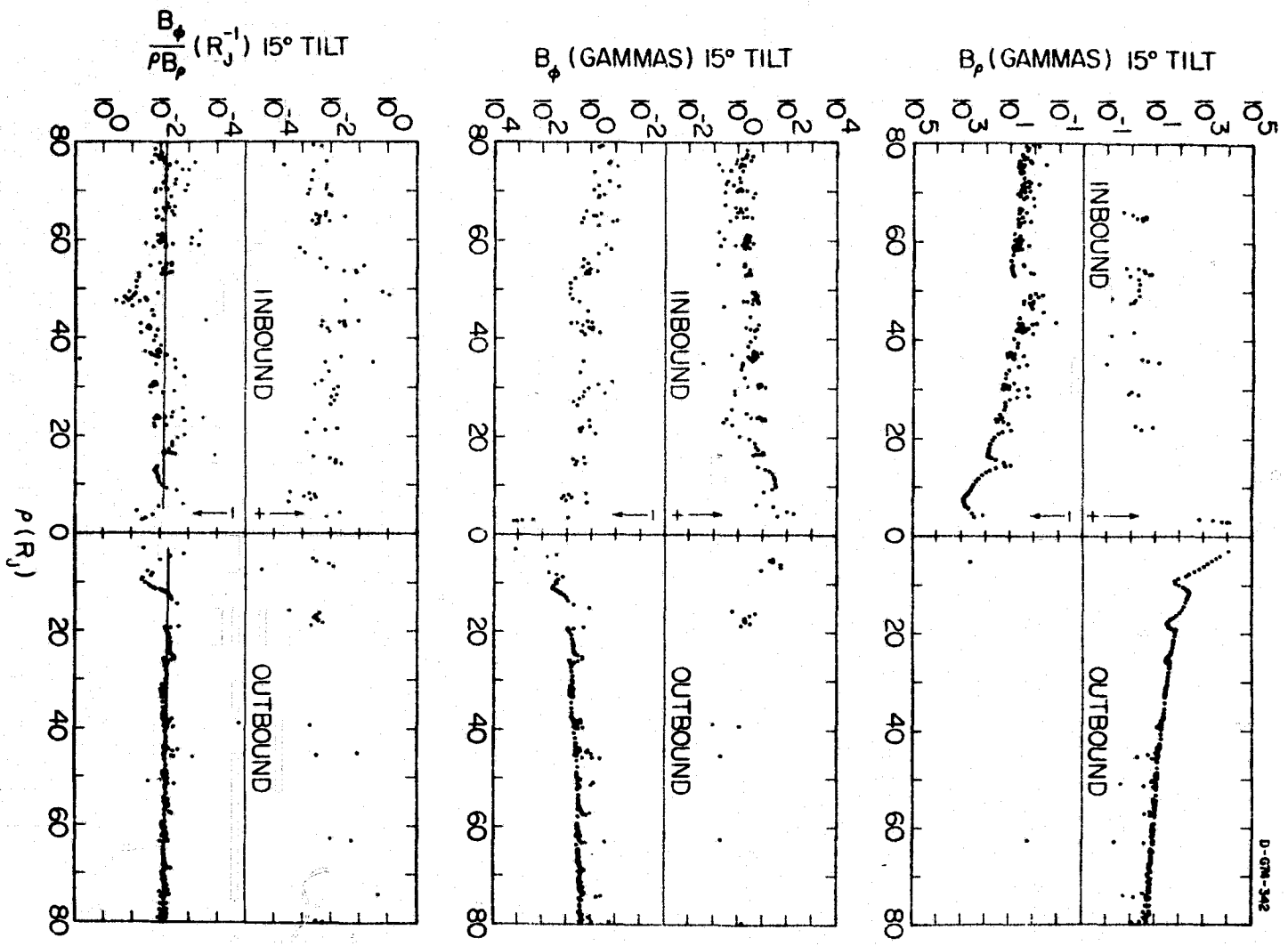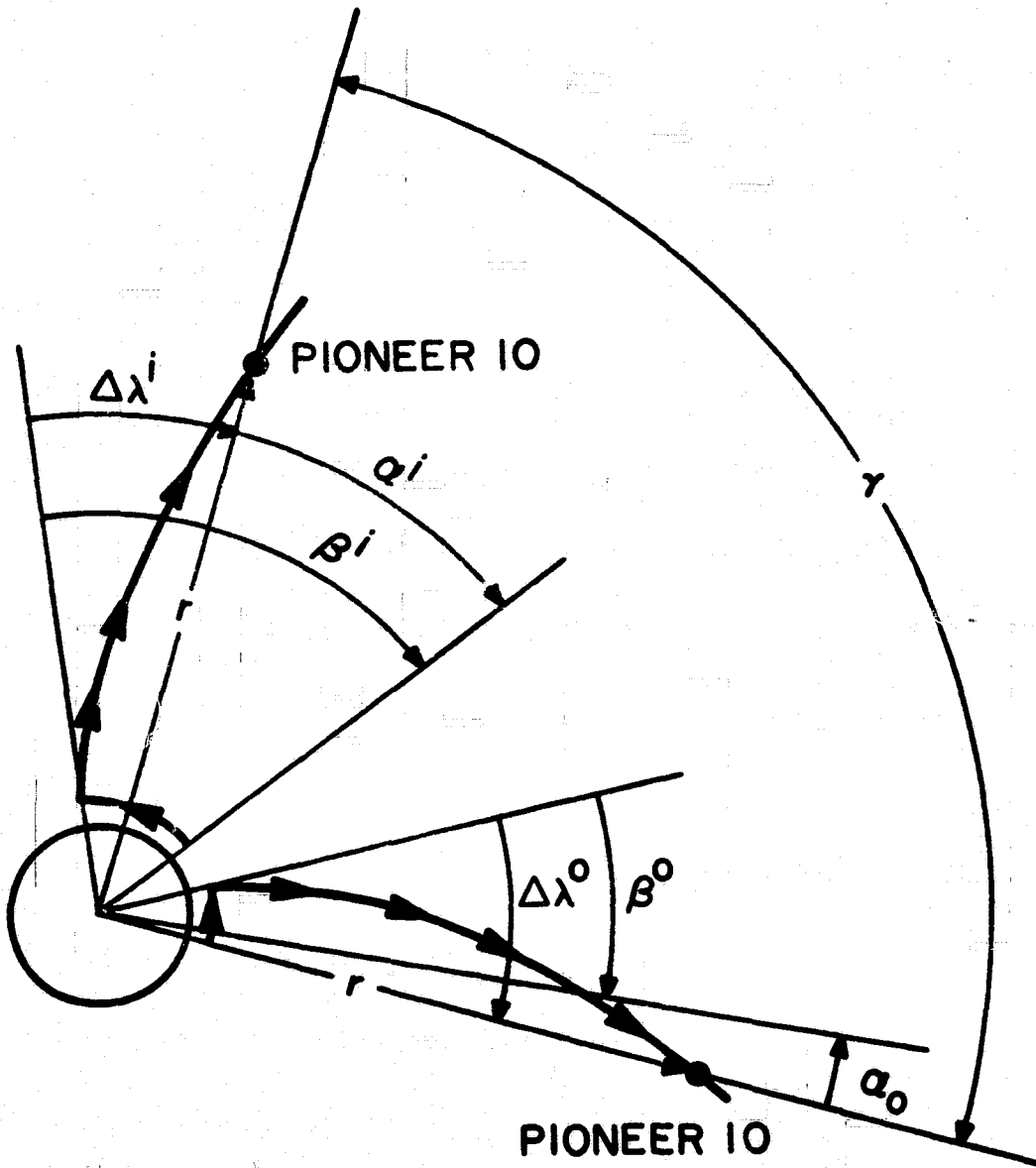A-674-344
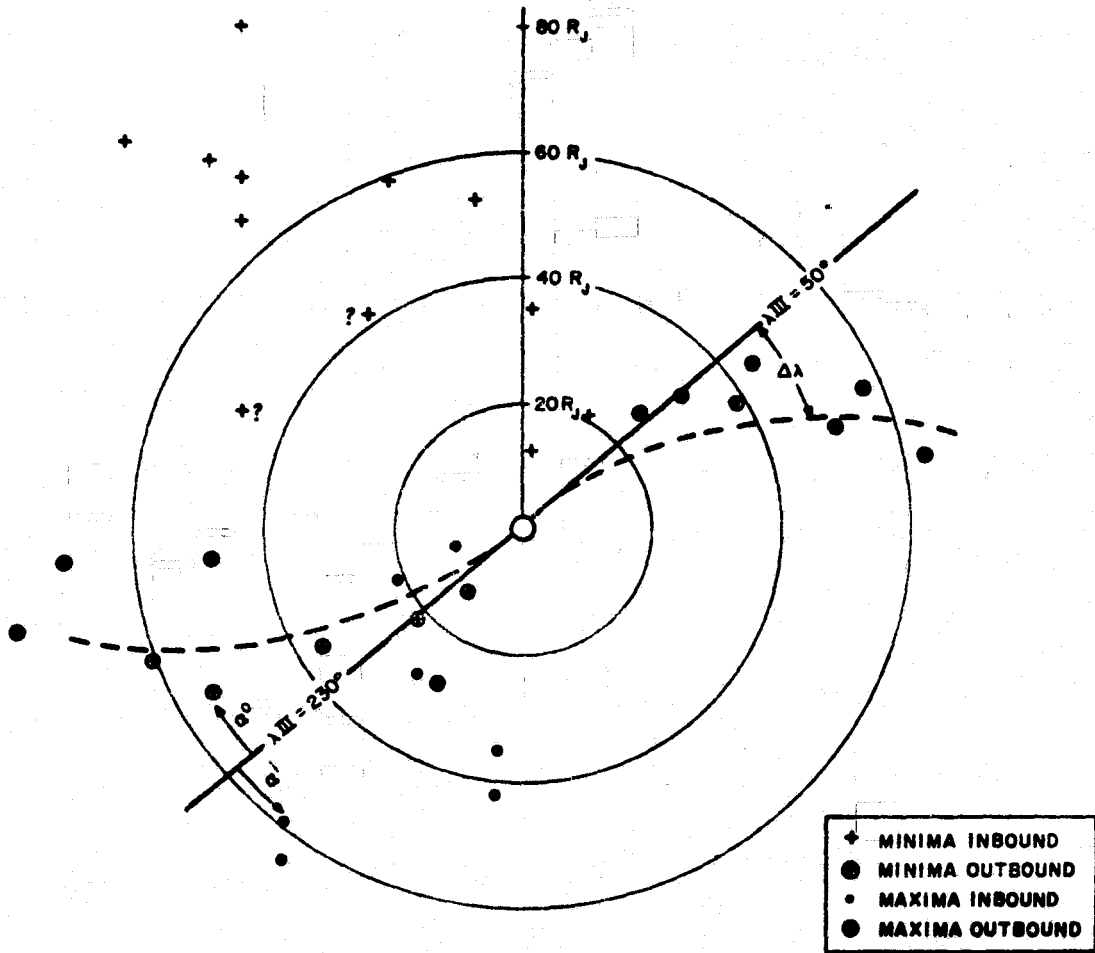
Figure 1

Figure 2

Figure 3

A-G74-345

Figure 4

The Magnetosphere of Jupiter as Observed with Pioneer 10.

Part III: Jovian Synchrotron Radiation at 10.4 cm as Deduced from Observed Electron Fluxes

T. G. Northrop[*]
Department of Physics and Astronomy,
University of Iowa, Iowa City, Iowa   52242

and

T. J. Birmingham
Theoretical Group, Goddard Space Flight Center,
Greenbelt, Maryland   20771

May 1974

[*]On leave from Goddard Space Flight Center.

ABSTRACT

Synchrotron radiation at 10.4 cm wavelength between 2.9 and

5.0 Jovian radii has been calculated from the electron fluxes observed

by the Iowa Pioneer 10 detectors. This calculated emissivity

(watts/m^3 x Hz x steradian) exceeds the Beard-Luthey [1973] spatial

resolution of the Berge [1966] interferometer measurements by about

a factor of 2 at 3 Jovian radii. The calculated emissivity is quite

insensitive to the energy spectral index. It is only moderately

sensitive to the equatorial angular distribution. The disagreement

would be only about 30% if Beard and Luthey had used the Iowa

angular distribution. A factor of 2 would represent a genuine

disagreement, but 30% would not exceed the combined uncertainties

of our analysis and the Beard-Luthey analysis.

INTRODUCTION

The University of Iowa detectors on Pioneer 10 give electron energy and angular distributions as functions of distance from Jupiter [Van Allen, et al., 1974]. We have used these measured distributions to calculate the emissivity (in watts/m^3 x Hz x steradian) of 10.4 cm wavelength radiation from the Jovian magnetic equatorial plasma. The emissivity is then compared to the radio astronomical observations from earth.

Berge [1966] has observed the decimetric synchrotron radiation at 10.4 cm as a function of distance from the planet. These measurements are unavoidably integrated along the line of sight through the Jovian magnetosphere. The emissivity per unit volume varies with radius, because both the magnitude of the field and the electron distribution vary. Beard and Luthey [1973] have resolved the Berge observations to give the volume emissivity of radiation polarized parallel to the magnetic dipole plane from a unit volume in the plane. Figure 1 shows their curve as well as the result of our calculations from the Iowa electron fluxes. Because Pioneer 10 did not penetrate to closer than 2.9 R_J (Jovian radii) the calculated curve does not extend inside of that radius. The discrepancy that appears between the Beard-Luthey curve and our calculation exceeds known possible errors in the data and calculations. At the end of

this paper we suggest a reason for the discrepancy.

RADIATION PER ELECTRON

The radiation emitted per steradian at right angles to the magnetic field $\vec{B}$ from harmonics in frequency range Δf (Hertz) and polarized perpendicular to $\vec{B}$ is [See for example Bekefi, 1966]

$$\Delta f \ \frac{e^2 \omega^2}{4\pi\epsilon_o c\omega_o} \ \beta_\perp^2 [J_m'(x)]^2 \ \text{(Mks units)}, \tag{1}$$

and polarized parallel to $\vec{B}$ is

$$\Delta f \ \frac{e^2 \omega^2}{4\pi\epsilon_o c\omega_o} \ \beta_\parallel^2 \ J_m^2(x) \tag{2}$$

where $\omega_o = \frac{eB}{m_o\gamma}$, m_o = electron rest mass, $\gamma = (1 - \beta^2)^{-\frac{1}{2}}$, ω = angular observation frequency ($\frac{\text{radians}}{\text{sec}}$), $m = \frac{\omega}{\omega_o}$, $x = \frac{\omega\beta_\perp}{\omega_o}$, $\beta_\parallel = \beta \cos \delta$, $\beta_\perp = \beta \sin \delta$, δ being the electron's pitch angle, and $J_m'(x)$ is the derivative with respect to x of the Bessel function $J_m(x)$. It has been assumed that there are many harmonics within Δf, a good approximation at 10.4 cm.

Usually $m \gg 1$; $m \geqslant 100$ for Jupiter and 10.4 cm wavelength. When m is large there is an approximation to the Bessel functions of

high order [Watson, 1922]

$$J_m(m \text{ sech } \alpha) \simeq \frac{\tanh \alpha}{\pi\sqrt{3}} e^{m(\tanh \alpha + \frac{1}{3}\tanh^3 \alpha - \alpha)} K_{1/3}(\frac{m}{3}\tanh^3 \alpha) ,$$

$$(3).$$

$K_{1/3}$ being the Bessel function of imaginary argument. For $\alpha < 1$, the

exponent in (3) is $-m[\frac{\alpha^5}{5} + 0(\alpha^7)]$; α is $\text{sech}^{-1} \beta_\perp$ in (1) and (2).

For the energies that contribute detectably to the radiation, γ

turns out to be greater than 10 ($\sim$ 5 Mev electrons) in the range of

2.9 to 5 Jovian radii. Because the half width of the radiation beam

of an electron is $\sim\frac{1}{2\gamma}$, electrons with pitch angles less than about

$\frac{\pi}{2} - \frac{1}{2\gamma}$ do not contribute to radiation perpendicular to $\vec{B}$. Thus,

$\beta_\perp \simeq 1 - \frac{3}{4\gamma^2}$ and $\alpha \simeq \frac{1}{\gamma}$. Thus, $\frac{-m\alpha^5}{5} \simeq \frac{-m}{5\gamma^5}$ is very small and the expo-

nential is unity for the purposes of this calculation.

Differentiation of (3) gives the expression for $J_m'(x)$ to be

used in expression (1), which then becomes

$$\Delta f \frac{e^2 \omega^2 \beta^4 \sin^4 \delta (\cos^2 \delta + \gamma^{-2}\sin^2 \delta)^2}{12\pi^3 \epsilon_o \ c \ \omega_o} K_{2/3}^2 \left[\frac{\omega\gamma}{(eB/m_o)} \frac{(\cos^2 \delta + \gamma^{-2}\sin^2 \delta)^{3/2}}{3} \right]$$

$$(4)$$

for the power radiated per steradian perpendicular to $\vec{B}$ and polarized

perpendicular to $\vec{B}$.

The omnidirectional flux of particles of energy greater than E was thus assumed to be (at the equator)

$$J(>E) = k(L) \ E^{-\Gamma(L)} \ , \tag{5}$$

where L is the number of Jovian radii from the center. The differential (in energy and pitch angle) flux corresponding to (5) is (in particles/m^2 x sec x steradian x Mev)

$$j(\delta,E,L,\lambda) = \frac{k(L) \ \Gamma(L)}{2\pi \ S(n)} \ E^{-(\Gamma+1)} \sin^{n}(E_\delta L) \tag{6}$$

where

$$S(n) = \int_{0}^{\pi} d\delta \ \sin^{n+1}\delta \ \simeq \ \sqrt{\frac{2\pi e}{n}} \ (\frac{n}{n+1})^{\frac{n+1}{2}} \tag{7}$$

the approximation being Stirling's and in error by less than 2% for n > 3. As indicated by the notation, the pitch angle distribution can in principle be a function of energy as well as of the radial distance, although the data obtained from only two passes through Jupiter's magnetosphere is insufficient to determine the dependence. Van Allen et al. [1974] have taken

$$n_C = 3.5 + (3.86/L)^8$$

$$\tag{8}$$

$$n_D = 4.0 + (3.57/L)^8$$

for the C and D detectors, respectively, as giving good closure between the inbound and outbound count rates (Figures 2 and 3). Because these detectors are energy integrating, $n_C \neq n$ (21 Mev, L) and $n_D \neq n$ (31 Mev,L), but are averages of some sort. We have used the average $\bar{n}(L)$ of $n_C(L)$ and $n_D(L)$ in the radiation calculation, and kept n independent of energy. Use of $\bar{n}$ does not introduce much error. Firstly, S(n) in (6) varies roughly as $\frac{1}{\sqrt{n}}$, as can be seen in (7) for n large. Secondly, the radiation integral (13) is totally insensitive to n, since the integrand goes to zero very rapidly away from $\delta = \frac{\pi}{2}$ because of the angular dependence of the $K_{2/3}^2$ factor, not because of the angular dependence of $\sin^{n+5}\delta$. The rapid cutoff by the $K_{2/3}^2$ is the mathematical manifestation of the narrow radiation beam of a relativistic electron. $\bar{n}$ decreases from 11.3 to 3.9 over the range L = 2.9 to 5.0.

The spectral index $\Gamma(L)$ is shown in Figure 4 and the coefficient k(L) in Figure 5. They were obtained from the C and D detector count rates as follows. Let

$$I(\Gamma) = \frac{\int_o^\infty dE \; R_C(E) \; E^{-(\Gamma+1)}}{\int_o^\infty dE \; R_D(E) \; E^{-(\Gamma+1)}} \; , \tag{9}$$

R_C and R_D being the count rates of the respective detectors per unit incident omnidirectional flux of electrons of energy E. Then $C(L)/D(L) = I[\Gamma(L)]$ is an integral equation to be solved for $\Gamma(L)$. $I(\Gamma)$ turns out to be given by $I(\Gamma) = 2.818\,e^{0.4032\,\Gamma}$ and therefore

$$\Gamma(L) = 5.711\,\lg_{10}\,[C(L)/D(L)] - 2.570\ . \tag{10}$$

The coefficient $k(L)$ is determined as follows: from (5)

$$-\frac{dJ(>E)}{dE} = k(L)\,\Gamma(L)\,E^{-(\Gamma+1)} \tag{11}$$

is the differential in energy flux. But

$$C(L) = \int_0^\infty dE\ R_C(E)\ \frac{-dJ}{dE} = k(L)\,\Gamma(L)\int_0^\infty dE\ R_C(E)\ E^{-(\Gamma+1)} \tag{12}$$

and $k(L)$ is determined because the integral is known from the detector calibration.

The curve $\Gamma(L)$ in Figure 4 indicates that the electron spectrum hardens as one comes in from L = 5, reaches a maximum hardness at about L = 3.6 and then softens. (The hump at L = 3.2 may be only an artifact of exactly how the C and D curves turn over inside L = 3.5.) The qualitative physical interpretation could be that of

a hardening of the spectrum caused by energizing of the electrons as they diffuse inward, followed by a selective sapping of the more energetic electrons as the radiation region is entered at about 3.5. In any case the radiated power is remarkably insensitive to Γ, as will be discussed below.

THE RADIATION

Multiplication of the radiation per particle (1) by the particle density j/c from (6) and integration over angle δ and energy E gives the total radiation from a unit volume per steradian at right angles to $\vec{B}$ and polarized $\perp \vec{B}$:

P(watts polarized $\perp \vec{B}/m^3$ x steradian x Hz) =

$$\frac{e^2 \omega^2 \ \Gamma(L) \ k(L) \ (0.511)^{-\Gamma}}{12\pi^3 \ \epsilon_o c^2 \ S[n(L)] \ (eB/m_o)} \int_o^\infty d\gamma \ \gamma^{-\Gamma} \int_o^\pi d\delta \ \sin^{n+5}\delta (\cos^2\delta + \gamma^{-2}\sin^2\delta)^2$$

$$\tag{13a}$$

$$K^2_{2/3}\left[\frac{\omega\gamma}{(eB/m_o)} \ \frac{(\cos^2\delta + \gamma^{-2}\sin^2\delta)^{3/2}}{3}\right]$$

$$= \frac{e^2 \omega 2 \ C(L)(0.511)^{-1} \ \int_o^\infty dE \ E^{-(\Gamma+1)} E \int_o^\pi d\delta \ \sin^{n+5}\delta (\cos^2\delta + 0.261 \ E^{-2} \sin^2\delta)^2 \ K^2_{2/3}[\ldots]}{12\pi^3 \ \epsilon_o c^2 \ [eB(L)/m_o] \ S[n(L)] \ \int_o^\infty dE \ E^{-(\Gamma+1)} \ R_C(E)}$$

$$\tag{13b}$$

the latter form upon substitution of k(L) from (12). The radiation integral in (13a) has been evaluated numerically. The Jovian dipole moment was taken as 4.0 gauss R_J^3 [Smith, et al., 1974]. Westfold's [1959] table of $K_{2/3}(x)$ was used with appropriate interpolation. Table 1 gives the % contribution to the total radiation of electrons in various energy ranges ($E \cong 0.511 \, \gamma$ Mev). The maximum contribution at each L is underlined. Clearly the contribution of electrons between 5 and 21 Mev is negligible except around L = 2.9, and even there the contribution cannot account for the discrepancy in Figure 1. The calculated radiation is insensitive to the extrapolation via $E^{-\Gamma}$ to energies below the C detector threshold of 21 Mev.

Table 2 illustrates the remarkable insensitivity to Γ. At each of the tabulated L's, the middle column is the radiation normalized to unity calculated for the "correct" Γ of Figure 4. The other two columns show how the calculated radiation would change for the same C(L), but increased or decreased Γ. Although the double integral in (13a) is very sensitive to Γ, so is the coefficient in a compensating sense. The explanation for the insensitivity is most easily visible in (13b), where all of the Γ dependence is in the integrals. If the ratio $E \int_0^\pi d\delta \, \ldots / R_C(E)$ were independent of E, the radiation would be independent of Γ. With the use of Table 1, it can be seen that at L = 2.9, $E \int_0^\pi d\delta \ldots$ increases from zero at about 10 Mev to a maximum at about 56 Mev and then falls off gently out

to $\gamma = 400$. On the other hand [Van Allen, et al., 1974] $R_c(E)$ increases in almost exactly the same fashion from zero at 10 Mev to a maximum at 60 Mev and remains constant at this maximum. The slight dependence on Γ at $L = 2.9$ arises from the slow fall off $E\int_0^\pi d\delta \ldots$ above its maximum. At L greater than 2.9, the Γ dependence increases because the maximum of the $E\int_0^\pi d\delta \ldots$ curve shifts to higher energies, as can be seen in Table 1.

CONCLUSIONS

In conclusion, it seems impossible to find enough latitude in the parameters of our calculation to reduce our results by the neces- sary factor of 2 or more to obtain agreement with the Beard-Luthey curve. However, about half of the disagreement would have disappeared if they had used our equatorial angular distributions (8). Lacking better information at that time, they assumed an isotropic distribu- tion in pitch angle from $\delta = 48°$ to $132°$. Distribution (8) is more concentrated in the equatorial plane than this, hence, produces more radiation from the equator. If they had used angular distribution (8), their resolved curve would have been higher by $\int_{48°}^{132°} d\delta \sin \delta /S(n) = 1.34/S(n)$. At $L = 2.9$ this factor is 1.92, while at $L = 3.5$ it is 1.42. This leaves our calculation some 30% above their result at $L = 3$, the % discrepancy increasing with L. We con- sider this much disagreement acceptable in view of the uncertainty

in their resolution of the low emission region at L > 3, and of uncertainties in our calculation. Pioneer 11 will penetrate the more intense region near L = 1.7 and permit a comparison where the Beard-Luthey curve is more reliable.

ACKNOWLEDGMENTS

Table 1

The % Contribution to the Total Radiation of Various Electron Energy Ranges (E ≅ 0.5 γ MeV)

	→A det		→C det	→D detector									
L	5-20	20-40	40-60	60-80	80-100	100-120	120-140	140-160	160-180	180-200	300-320	380-400	←γ
2.9	0.01	13.6	32.6%	22.0	12.2	6.9	4.1	2.6	1.7	1.2	0.2	0.1	
3.5	0.00	2.0	18.4	23.6%	17.6	11.7	7.7	5.2	3.6	2.6	0.5	0.2	
4.0	0.00	0.3	8.5	19.7	19.2	14.6	10.3	7.2	5.1	3.7	0.8	0.4	
5.0	0.00	0.0	0.8	7.3	14.8	16.3	14.1	11.2	8.5	6.4	1.4	0.7	

Table 2

Sensitivity of the Radiation to Γ

L	Using $\Gamma - 0.2$	Radiation Using Correct Γ	Using $\Gamma + 0.2$
2.9	0.97	1	0.97
3.5	1.05	1	0.94
4.0	1.09	1	0.88
5.0	1.18	1	0.83

REFERENCES

Beard, D. B. and J. L. Luthey, Analysis of the Jovian electron radiation belts, 2, Observations of the decimetric radiation, Astrophys. J., 183, 679, 1973.

Bekefi, G., Radiation Processes in Plasmas, Ch. 6, John Wiley, New York, 1966.

Berge, G. L., An interferometric study of Jupiter's decimeter radio emission, Astrophys. J., 146, 767, 1966.

Smith, E. J., L. Davis, Jr., D. E. Jones, D. S. Colburn, P. J. Coleman, Jr., P. Dyal, and C. P. Sonnett, Magnetic field of Jupiter and its interaction with the solar wind, Science, 183, 305, 1974.

Van Allen, J. A., D. N. Baker, B. A. Randall, and D. B. Sentman, The magnetosphere of Jupiter as observed with Pioneer 10. Part I: Instrument and principal findings, J. Geophys. Res., [1974], accompanying paper.

Watson, G. N., A treatise on the theory of Bessel functions, Cambridge University Press, 1922.

Westfold, K. C., The polarization of synchrotron radiation, Astrophys. J., 130, 241, 1959.
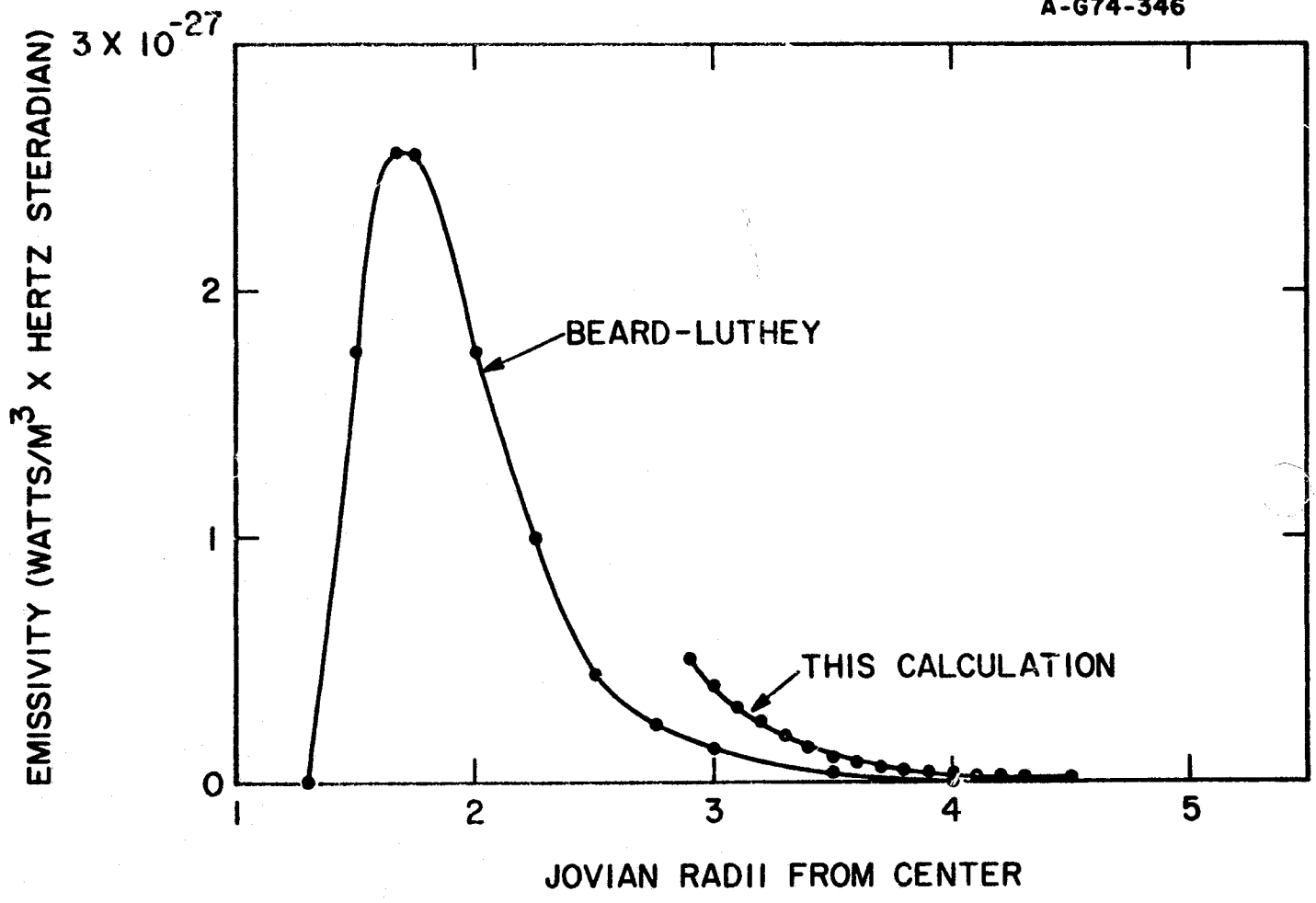
FIGURE CAPTIONS

Figure 1. Emissivity of 10.4 cm radiation polarized parallel to the magnetic equator, as calculated from the electron fluxes and as deduced by Beard and Luthey from the Berge interferometer measurements.

Figure 2. Counting rate of the Iowa C electron detector (energies > 21 MeV) corrected to the magnetic equator for the inbound and outbound passes.

Figure 3. Counting rate of the Iowa D electron detector (energies > 31 Mev) corrected to the magnetic equator for the inbound and outbound passes.

Figure 4. The integral (in energy) power law spectral index Γ.

Figure 5. The coefficient k(L) appearing in the integrated (in energy and angle) flux $k(L) \, E(Mev)^{-\Gamma(L)}$.
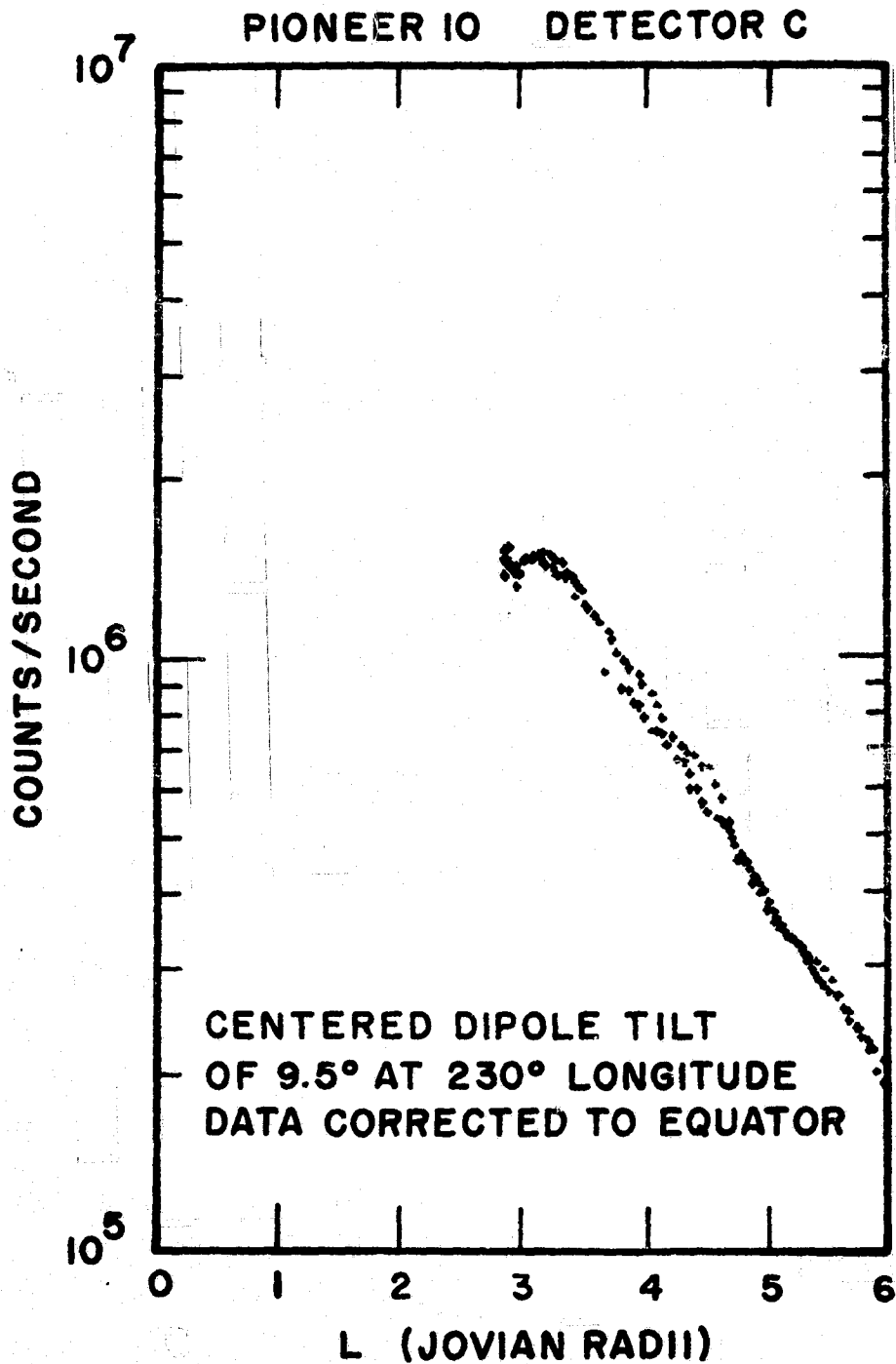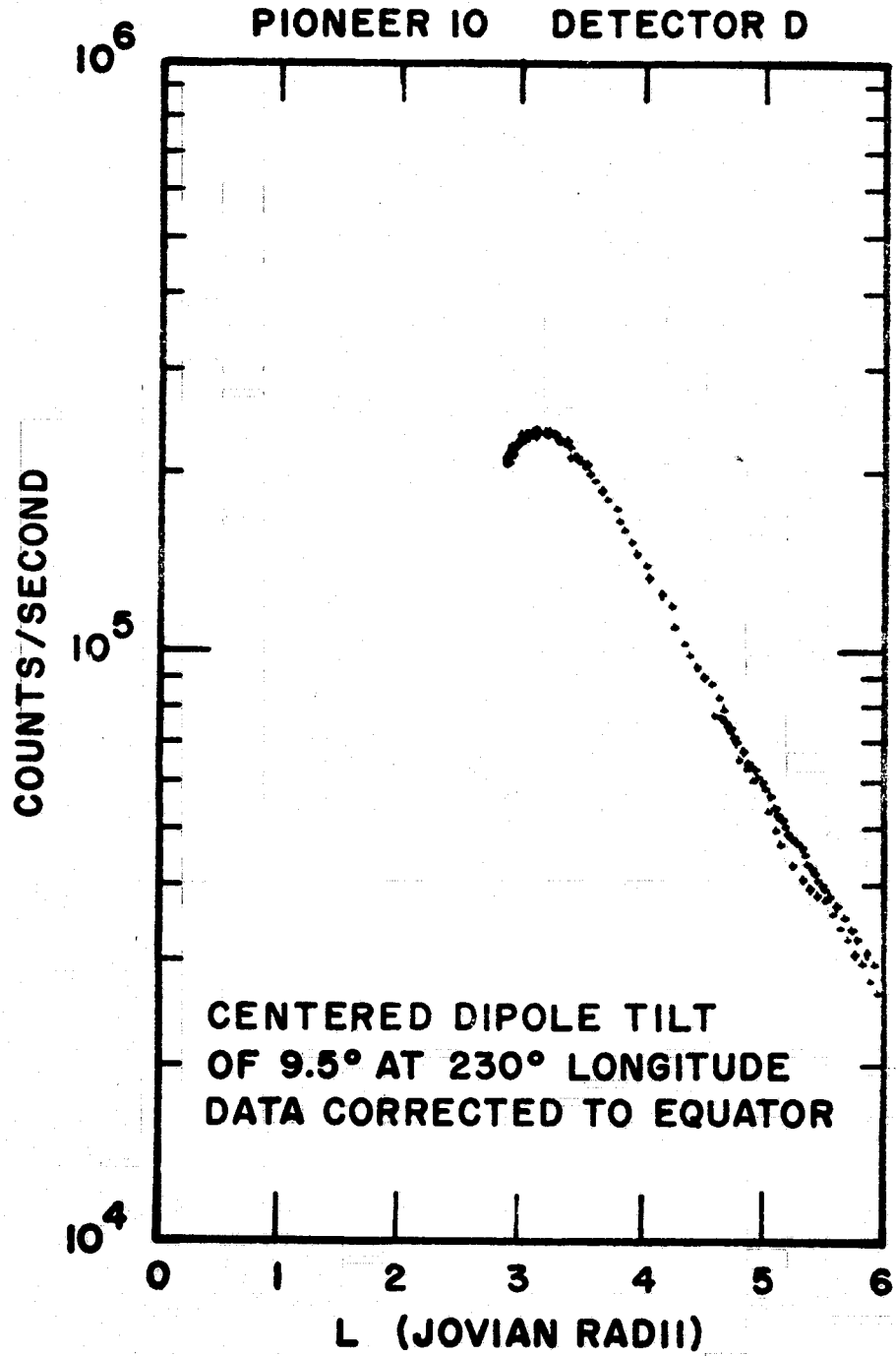
Figure 1

Figure 2

A-G74-338-1

Figure 3

Figure 4

125<

Figure 5